University of Stavanger

Faculty of Science and Technology

MASTER'S THESIS

Study program/Specialization: Petroleum Engineering/Drilling	Spring semester, 2016 Open
Writer: Kristoffer Rage	…… (Writer's signature)
Faculty supervisor: Remi-Erempagemo T Meindinyo, Thor Martin Svartaas External supervisor:	
Thesis title: Analysis of Gas Hydrate Growth Models	
Credits (ECTS):	
Key words: Hydrates of natural gases Gas hydrate Hydrate growth Gas hydrate model Analysis	Pages: 87 + enclosure: 10 Stavanger, 28.06/2016 Date/year

ABSTRACT

The kinetic behaviour of gas hydrate formation of pure methane have been studied and predicted based on different models. Experiments have been conducted at different temperatures and stirring rate, and the measured results have been closely examined and compared to the results produced by the models.

The experimental setup used in this thesis consist of a stirred cell reactor with a volume of 141.4 ml and with inner diameter of 60 mm, outer diameter of 90mm and a height of 50 mm. The cell is connected to a high pressure methane tank using a pressure reduction valve and a flow meter while being operated in open mode as to allow constant pressure supply of gas for the duration of the experiment.

Experiments were ran at 6, 7 and 8 ˚C and at stirring rates from 225 to 800 rpm. 50 ml of distilled water was used for all of the experiments.

The measured data on gas consumption, based on the amount of gas passing through the flow meter, as well as the heat released was used to estimate the hydrate growth rate. The start of each experiment is indicated by a rapid increase of temperature and gas consumption, and the end by the rotor blade either getting stuck in the hydrates, or reaching a constant power consumption due to pushing the hydrates aside. The growth period could be divided into three different growth stages, stage 1 representing the initial growth phase, stage 2 the mid-section and stage 3 the final section. Within each of this stages the growth rate can be approximately represented by a linear growth rate. The main focus in this thesis lies on growth stage 2.

Nomenclature

P	absolute pressure, bar
T	absolute temperature, ˚C, K
H	enthalpy
ΔH	change in enthalpy
c_p	heat capacity
Δgv	free energy per unit volume
T_{eq}	hydrate equilibrium temperature, ˚C, K
t	time, min, s
t_{onset}	time of initial hydrate detection, time from start of stirring, min
HON	homogeneous nucleation
HEN	heterogeneous nucleation
PBE	population balance equation
PDE	population distribution equation
w	water
g	gas
HC	hydrocarbon
sI	structure I
sII	structure II
sIII	structure III
σ	surface tension between liquid and crystal, mN/m
σ_w	interfacial
r_c	critical radius
θ	contact angle between surface and hydrate crystal

ΔG_{crit}	critical Gibbs free energy required for spontaneous nucleation for HON
$\Delta G'_{crit}$	critical Gibbs free energy required for spontaneous nucleation for HEN
φ	fraction between ΔG_{crit} and $\Delta G'_{crit}$
W(J)	work required to form hydrate cluster
$\Delta\mu$	supersaturation
C	shape factor
v_h	volume of hydrate build units, m^3
σ_{ef}	effective specific surface energy, J/m^2
f	fugacity of methane
f^{eq}	fugacity of methane at equilibrium
f^{b}	fugacity of methane in the liquid bulk phase
f^{exp}	fugacity of methane at experimental pressure
Δg^{exp}	total molar change in Gibbs free energy
pr	products
rx	reactants
exp	experimental
R	gas constant, 8,314, J/Kmol
A_p	surface area of particle, m^2
k_r	reaction rate constant
k_d	mass transfer coefficient around the particle
K*	growth rate of hydrate, fitted parameter
μ_2	second moment of particle size distribution
μ_0	number of hydrate particles per unit of liquid volume
r	radius of particle

$\varphi(r,t)$	crystal size distribution
D	diffusivity of gas
C	concentration of gas
y	distance from gas-liquid interface
H	Henry's constant
c_{wo}	initial concentration of water
y_L	film thickness
γ	Hatta number
$A_{(g-l)}$	total gas-liquid interfacial area
a	interfacial area per unit of liquid volume
M	molecular weight of hydrate
ρ	density of hydrate
N_p	initial number of hydrate particles
V_L	total liquid volume
n_{tb}	number of moles of hydrate at the turbidity point
n_{eq}	number of moles of hydrate at equilibrium
v_{hyd}	molar volume of hydrate
n_w	number of water molecules per gas molecule in the hydrate
v_w	molar volume of water
N	speed of agitation
Vg	volume of gas
Vl	volume of liquid
dI	diameter of impeller
dT	diameter of tank

h1 height of impeller

h2 height of water

x_{int} mole fraction of gas in the water phase at the water-gas interface in equilibrium with gas phase at the system pressure and temperature

x_b mole fraction of gas in the bulk water phase at the water-gas interface in equilibrium with gas phase at the system pressure and temperature

z gas compressibility factor

Po Power, W

M_w molar mass of water

ρ_w density of water

n_{GC} moles of gas consumed

f_w water fraction

f_h hydrate fraction

μ_B viscosity of water

V_A molar volume of methane, cm^3/mol

M_B molar mass of methane

ϕ association factor for water

α_2 nucleation constant, $nuclei/m^2s$

η_L liquid viscosity

ε energy dissipation rate per unit mass of fluid

B Hamaker constant of methane hydrate in water

$\lambda(\sim r, r^*)$frequency of agglomeration between particles of radius ~r and r^*

E(r) net contribution of birth/death terms due to crystal aggregation

Q(r) net contribution of birth/death terms due to crystal breakage

TABLE OF CONTENTS

PREFACE

The year was 2011 when I first set foot on the University of Stavanger campus. Fresh out of Upper Secondary School at Tryggheim Skular, with big ambitions and an ever growing will to learn. The subject I chose back then was a 3 year Bachelor in Petroleum Technology.

After finishing the Bachelor in 2014, I found myself still wanting to know more about the field of Petroleum, and therefore applied for a Master's degree with a specialisation in drilling. I was accepted, and noticed quickly a rapid increase in both difficulty, but also everything was more interesting and fun to learn about.

Finally, the last semester of my Master's degree was quickly approaching, and I reflected back on what had interested me the most during my stay at the University. The first thing that came to mind was working on something related to improving oil recovery, but as a result of many drilling students and few drilling teachers, I ended up writing about natural gas hydrate, and the models describing them no less!

The learning curve was steep, as I had limited back ground on the subject. This fact, I think, only made the experience even more satisfying once I finally finished. Looking back, it was both a stressful and very educating experience all together.

I would very much like to thank my supervisor Remi-Erempagamo T Meindinyo for patient and helpful guidance throughout the process of writing of the thesis and the all the work at the lab for this thesis. Without your help, this thesis would be nearly impossible to complete.

Secondly, I'd like to thank Thor Martin Svartaas for being very enthusiastic and helpful towards answering any of my questions regarding everything from lab procedures to chemical properties of methane gas.

Third and final thanks goes to bachelor student Kristina Kroknes, who assisted me in some of my lab experiments, as well as conducting some of her own and sharing her data. We had a very enjoyable time working together.

1. INTRODUCTION

1.1. Background knowledge

Natural gas hydrate are quite like ice, as in frozen water, but can be generated at temperatures above zero degrees Celsius at atmospheric pressures. This is made possible due to van der Waal's forces that stabilize the solid crystal structures in the hydrates. Gas molecules, also known as the guest, are caged in water molecules bound together by hydrogen bonds. These are water molecules are called the hosts. Methane, ethane, propane and carbon dioxide are the most common guests (Sloan Jr & Koh, 2007).

Gas hydrates was first discovered in 1810 by Sir Humphry Davy (Davy & Bulmer, 1810). At first, hydrates were for the most part considered to be a laboratory curiosity. That changed rapidly when they turned out to be responsible for the plugging of natural gas flowlines in 1934 by Hammerschmidt (Hammerschmidt, 1934). At this point, there was a need for more understanding of the concept, and an intense study of the thermodynamics of hydrate formation ensued. The result was the development of reliable models that may be used to calculate the phase equilibria, as well as thermodynamic inhibitors of hydrate formation, e.g. methanol and glycols (Ribeiro & Lage, 2008). These inhibitors are used to prevent formation of hydrate plugs in petroleum flowlines, a problem which along with safely removal of hydrate plugs represent 70% of the deepwater flow assurance challenges of the petroleum industry (PetroWiki, 2015).

Normally about 85% of the weight percent in hydrates will be composed of water molecules, while the remaining will be gas. This is in fact quite dense for gas, considering it can be can be stored this way without the need of high pressures, which possibly makes this a safer option than compressed gas, in terms of gas storing. One volume of hydrate can contain up to 184 volumes of gas at standard conditions. This makes it an ideal option for either storing or transportation of gas, or even disposing of unwanted gas, such as carbon dioxide. It also makes it an unconventional energy resource considering the fact that rather large quantities of gas are already naturally stored this way around the globe. There's estimated to be world-wide reserves of roughly $0.2 * 10^{15}$ - $120 * 10^{15}$ m^3 of methane (STP) (Sloan Jr & Koh, 2007).

The biggest hindrance for these potential applications of hydrates comes from the slow formation rate, economics of scale up and low conversions. Our best bet to overcome these challenges is to obtain a better understanding of the hydrate formation kinetics, which unlike thermodynamics, are still in the dark (Ribeiro & Lage, 2008).

When hydrates are formed, measureable heat is released to the surrounding. This means that the formation of gas hydrates is an exothermic process. In other words, it is possible to detect it by detecting the heat transfer, and the energy released in terms of enthalpy can be measured. Gas consumption can also be measured if the reaction happens in a closed environment, like in a lab trial. These variables are paramount in some of the different gas hydrate models used today (Sloan Jr & Koh, 2007).

1.1. Definition of thesis

This thesis is based on an analysis of models describing different aspects of clathrate hydrate growth and comparing these with experimental results. Experiments will be conducted at the University lab by myself, but data from other current and previous students will also be takin into consideration when applicable. The experiments will measure gas consumption rate using a flow meter, while also documenting everything from temperature in water and gas phase within the cell, the stirring rate, the power consumption of the stirring blade and the pressure inside the cell. The aim of this master's thesis is to determine whether or not the analysed models can be used to predict hydrate growth rate within the reaction cell. The focus will be on two of the first and best known models we have today, presented by Englezos et al. and Skovborg and Rasmussen respectively.

In the following studies, experiments were conducted using one component gas, methane, and pure distilled water.

2. THEORY

2.1. Structure

Depending on the size of the guest molecule, the water molecules will arrange in different structures. For the vast majority they will form in one of the following structures (Sloan Jr & Koh, 2007):

- Structure I (sI) if the diameter of the guest molecule is between 4.2 and 6 Å.
- Structure II (sII) if it is smaller than 4.2 Å or between 6 and 7 Å.
- Structure H (sH) if it is between 7 and 9 Å.

The existence of structure I and II was first confirmed between the late 1940s and early 1950s by von Stackelberg et al. when they released a summary of their work (1954a, 1954b). Here they showed a series of x-ray experiments concerning crystal diffraction, which lead to the determination of the two first structures (Sloan Jr & Koh, 2007).

Structure H was later discovered by the use of nuclear magnetic resonance (NMR) by Ripmeester et al. (1987). In addition to this there was discovered another five structures by Jeffrey (1984), III – VII. (Sloan Jr & Koh, 2007) But since none of these have been found to contain any hydrocarbon guests, they will for the most part be disregarded for this thesis.

These structures are by themselves not in a stable form because of repulsive forces between the lattices. However, the structure is stabilized by the trapped guest molecule in the middle, i.e. the gas molecule. Visually the hydrates share an appearance with ice or snow, but their properties differ quite a bit. As previously mentioned, hydrates can form at temperatures much higher than ice, and while ice may form as a pure substance, hydrates cannot. In order for there to be hydrate formation, there needs to be both water and gas present, along the correct conditions of course (Sloan Jr & Koh, 2007).

The most stable hydrate structure is the tetrahedral bond, which have angles of 109.5 degrees. As suggested by Stillinger (1980) (Rowland & Stillinger, 1980), this is the best way of packing molecules, with fully developed hydrogen bonds, along with almost no geometrical distortion (Sloan Jr & Koh, 2007).

2.2. Cavities

Cavities is the open space that forms between the bonded molecules that together make up the lattice in the hydrate formation. When it comes to hydrates, there is a specific nomenclature that is used to differentiate the different configurations, which was originally created by Jeffry (Jeffrey, 1984). Here, the different configurations are described using the format n_i^{mi}. Ni tells indicates the number of edges in the "i" face type, and *mi* the number of faces there is with ni edges (Sloan Jr & Koh, 2007).

For example, one of the more simple configurations, namely the pentagonal dodecahedron, which is the small cavity in hydrate structures. This cavity is labelled 5^{12} using the nomenclature, because it has 5 edges and 12 pentagonal faces. Another configuration, the tetrakaidecahedron, which is a large cavity in sI. This cavity is labelled $5^{12}6^2$, which means 12 pentagonal faces of 5 edges, and 2 hexagonal faces with 6 edges (Sloan Jr & Koh, 2007).

There is also the 16 sided cavity, or $5^{12}6^4$ also known as hexakaidecahedral, usually seen in sII as a large cavity. This consist of 12 pentagonal faces, and 4 hexagonal. The $4^35^66^3$ dodecahedron is quite irregular when compared with the previously mentioned, as it consist of 3 different sizes of faces, i.e. 3 squares, 6 pentagonal and 3 hexagonal faces. This is often the medium sized cavity in sH. Finally there is the $5^{12}6^8$ icosahedron, which is the largest of the ones that have mentioned. It has 12 pentagonal faces a d 8 hexagonal, and is found as a large cavity in sH (Sloan Jr & Koh, 2007).

In order to define a suitable size of a guest molecule in a certain structure, one can use the method suggested by Davidson (Davidson, 1973) where the van der Waals radius of the water molecule is subtracted from the average cage radius of the different cage configurations present. When calculating the lower and upper boundaries for a suitable guest molecule, one should consider the diameter ratios of a single hydrate former, or a single compound. The lower boundary is equal to 0.76 of the average cavity diameter, and the upper is equal to 1.0. If the guest molecule is below the lower value, then it will be too small to be able to stabilize the structure, and if it is above the upper value, then the cavity will be stretched and create strains.

Regardless, any structural type depends on the hydrate former and the size of it. That is, a gas mixture or a pure gas at a specific temperature and pressure to make a particular structure. The small cavities in the different structures are often all the same, which means that many of the same components can be found in different structures. In other words, the structural type is primarily decided by which hydrate former, or gas composition, that are found within the large cavities. (Sloan Jr & Koh, 2007)

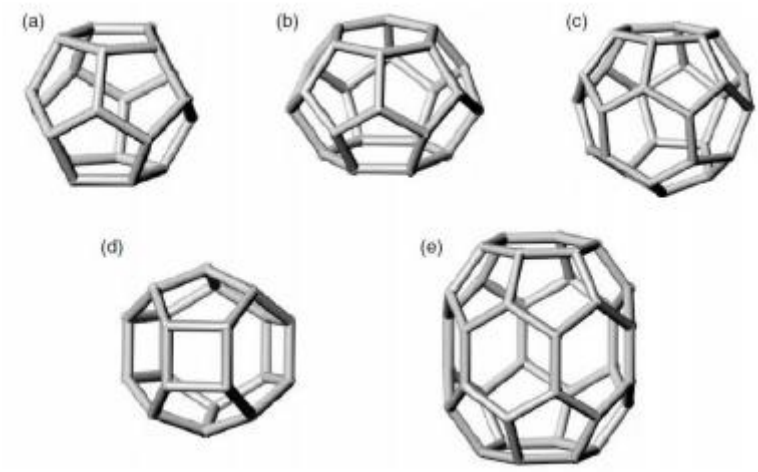

Figure 1: Cavities in gas hydrates. (a) pentagonal dodecahedron (5^{12}), (b) tetrakaidecahedron ($5^{12}6^2$), (c) hexakaidecahedron ($5^{12}6^4$), (d) irredular dodecahedron ($4^3 5^6 6^3$), (e) icosahedron ($5^{12}6^8$) (Sloan Jr & Koh, 2007)

2.3. Structure I

Structure I, or sI, is the simplest form a hydrate can take. It is a cubical shape, and consist of 5^{12} and $5^{12}6^2$ structured cavities. Here, the dodecahedron (5^{12}) serves as the small cavity and contains 20 water molecules and has a radius equal to 3.95 Å. The most common guest molecules present in this structure is Xe, CH_4, H_2S as well as more gas molecules that are non-polar under normal pressures and temperatures. The large cavity, the tetrakaidecahedron ($5^{12}6^2$), has 24 water molecules and radius equal to 4.33 Å. As for the guest molecules found within the large cavity, the majority will be methane CH_4 and/or ethane C_2H_6. As one may have noticed, methane can occupy both the large and the small cavity, while ethane will stick to only the large ones. Two small and six large cavities together with 46 water molecules arranged as lattices around the cavities make up for the composition of sI. One of the

trademarks of this structure is that it will be unable to form if the guest molecules are larger than propane.

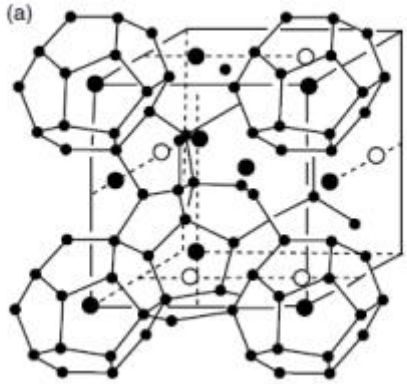

Figure 2: An illustration of hydrate crystal unit for sI (McMullan & Jeffrey, 1965).

2.4. Structure II

This is the most common structure found in the petroleum industry. It is similar to sI in that it is also a cubical shape, however, sII is a lot more complex. The composition is small and large cavities, where the small ones are the same as in sI and sH, as in dodecahedron. The only difference is that in sII the average radius of the small cavity is equal to 3,91 Å, not 3,95 Å as in sI. This is most likely the reason why pure nitrogen gas, N_2, forms sII, and not sI, as it would be able to stabilize the cavity better. With regards to the large cavity in sII there is the hexahaidecahedron, or $5^{12}6^4$. This is somewhat larger than that of sI, with an average radius of 6,6 Å. This means that the cavity can host guests of larger size than those in sI, such as propane and iso-butane. In sII there is a lot more cavities. A total of 24, where 16 are small and 8 are large. Despite the fact the the average radius of dodecahedron is somewhat lower for sII, the number of water molecules per cavity is still the exact same. Creating the lattices around these 24 cavities are a total of 136 water molecules.

2.5. Structure H

This is the least common of the first three hydrate structures. It has a hexagonal shape, as denoted by the H. unlike sI and sII, this structure has three different sized cavities, small, medium and large, as well as requiring two guest molecules to be stabilized. The small and medium sized cavities can be stabilized by a small to medium sized gas, and the large cavity require a large guest. The small, medium and large cavities are respectively dodecahedron (5^{12}), irregular dodecahedron ($4^3 5^4 6^3$) and icosahedron ($5^{12}6^8$). The large cavity has a radius equal to 5,79 Å, something which allows for rather large quest molecules. Among these are the 2-methylbutane, 2,2-dimethylbutane, 2,3-dimethylbutane, 2.2.3-trimethylbutane and cyclooctane. These are for the most part not found in natural gas reservoirs, something which might explain why structure H is so rare to come across in oil and gas flowlines (Sloan Jr & Koh, 2007).

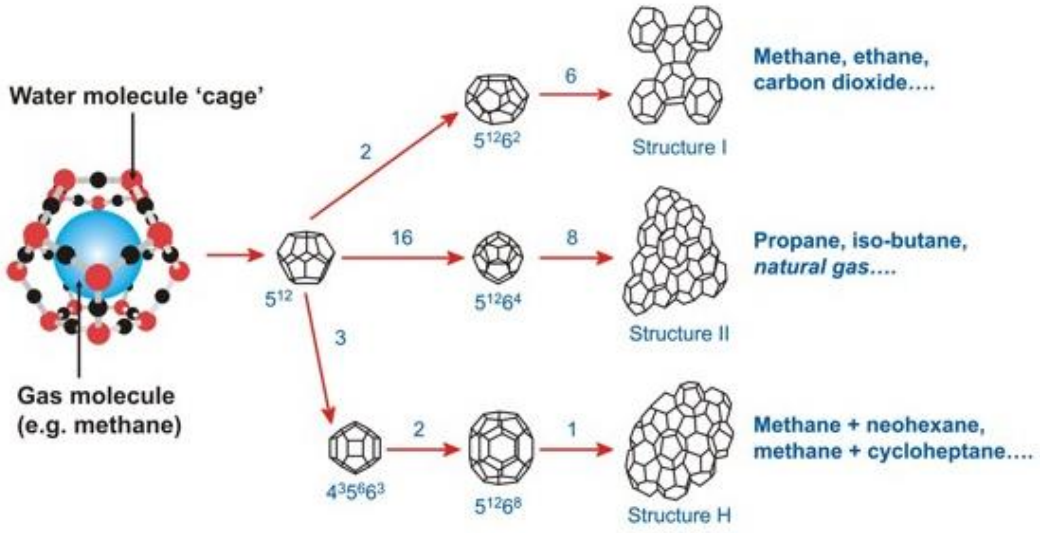

Figure 3: The different hydrate structures (Tohidi, 2011).

2.6. Enthalpy

Enthalpy is an expression of temperature change in a process, symbolized by H. any system has a constant or given enthalpy. However, when there is a chemical reaction or a change in temperature, internal energy, the enthalpy of the system will be changed accordingly, either

due to added heat, or lost or produced heat. The change in enthalpy, ΔH, of such a reaction is expressed as:

$$\Delta H = H_{pro} - H_{reac} \quad (1)$$

Where H_{pro} represent the enthalpy of the products, and H_{reac} of the reactants. As a definition, the formation enthalpy of elements in their natural state is set to be zero.

Heat capacity at constant pressure, c_p, is defined as:

$$c_p \equiv (\frac{\delta H}{\delta T})_p \quad (2)$$

When heat is released, the process is called an exothermic reaction and the change of enthalpy, $\Delta H < 0$. When the process required energy input, or heat input, it is called endothermic, and $\Delta H > 0$.

In the case of adiabatic processes without any heat loss to the surroundings all the energy released will be stored in the volume and the enthalpy change can be determined directly from the temperature change in the product and the heat capacity of it. When there is heat loss in a process, one can estimate the enthalpy of the formation if the heat loss rate is known.

Several studies has been conducted on the formation enthalpy of different hydrate systems at several different temperature conditions and gas compositions. Lievois wrote in 1987 a PhD thesis on the matter (LIEVOIS, 1987) which provided some results based on his experiments on formation enthalpy with pure methane.

2.7. Solubility

Solubility is a property of a solid, liquid or gaseous substance, also known as a solute, and it is an indication of a solute's ability to dissolve in a given solvent. This solubility is dependent on the physical and chemical properties of both the solute and the solvent, as well as the temperature, pressure and pH of the solution. The extent of the solubility can be measured as the amount of solute that can be dissolved into a solvent before adding more will no longer result in increasing concentration, but instead the solution begins to precipitate.

In this thesis the focus is on how much methane can be dissolved in distilled water under experimental condition. At normal condition, methane gas is not very soluble in water, but as pressure increases and temperature drops, this value will start to increase. Considering the fact that methane is probably one of the most important gases found in nature, there is a very limited amount of published data around methane solubility. And on top of this, the data that is available is of rather poor quality. There are some models proposed, such as the one by Duan and Mao (Duan & Mao, 2006) which to some reliable degree can predict the solubility of methane in was both in pure and saline solutions. However, as stated in the paper, these models cannot be used to predict solubility in the presence of hydrate. This becomes a challenge, since the experiments in this thesis revolves around hydrate. This will be further discussed in the result section.

2.8. Nucleation

The nucleation process is by far the most difficult to predict when it comes to how hydrates form, dissociate and are inhibited with time. The phenomenon is considered a stochastic process. This makes it very hard to observe at the actual point of nucleation, as well as the rate of growth. When hydrates are concerned, it is advised to pay attention to the driving force of the reaction. Hydrates prefer low temperatures and high pressures, when this driving force is low, the observed values are highly stochastic, and when the driving force is high then the value distribution is less so (Sloan Jr & Koh, 2007).

When it comes to the actual process of nucleation, it is explained as small clusters of water and gas, also known as hydrate nuclei, grow and then disperse, all in an attempt to achieve what is called a critical size. When this point is reached, the nuclei will be able to continue to grow, and the hydrate is formed. This is a microscopic phenomenon which may contain up to thousands of molecules, something which makes it very challenging to detect my experimental means. The hypothesis currently available for nucleation is based upon the principals of normal water freezing, dissolution of hydrocarbons in water as well as computer simulations that are based on both. When talking about the metastable region, one usually refers to the region where molecules nucleate and dissociate, without actually reaching the critical point. (Sloan Jr & Koh, 2007)

2.9. Homogenous Nucleation (HON)

Homogenous nucleation is something that does not happen very often in the real world. Even so, regardless of some of its shortcomings, the classical nucleation theory by Volmer and Weber in 1926 (Volmer & Weber, 1926) is still in use as a basis for most of our modern treatments of nucleation. (Sloan Jr & Koh, 2007) Because of this, only a short explanation of the concept of homogenous nucleation will be included in this thesis.

Basically, homogenous nucleation is a solidification process that happens when there are no impurities present. The process involves a lot more molecules than could possibly collide at the same time, so it is more likely that a sequence of bimolecular collisions of autocatalytic nature is introduced. What this means, is that there is a formation of clusters within the liquid that grow in size until a critical size is achieved. This size is known as the size at which the nuclei can grow spontaneously. (Sloan Jr & Koh, 2007)

Prior to reaching this critical size, the clusters of molecules will form in the bulk metastable liquid, where they will either grow or shrink depending on density and fluctuations in the composition. When the cluster finally reaches the critical size, a monotonic growth will occur. See figure below for an illustration.

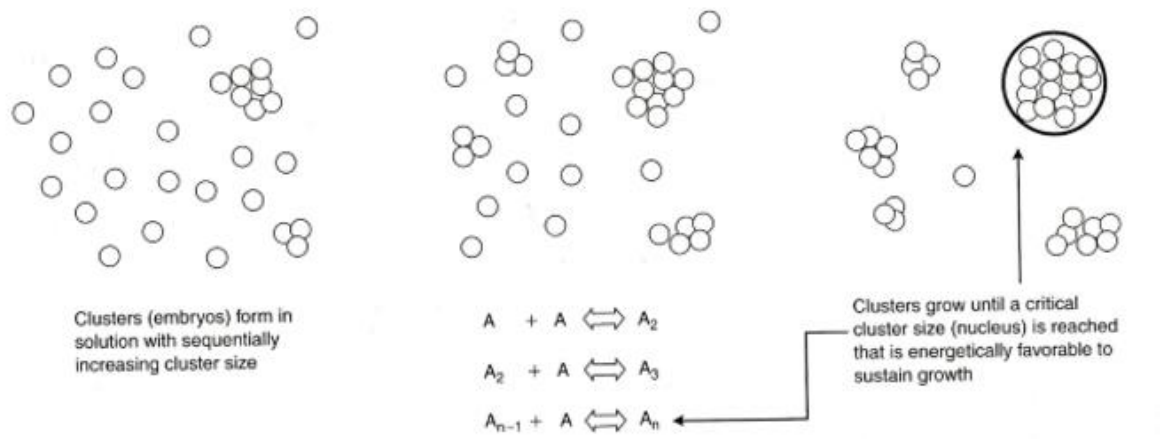

Figure 4: Illustration of the formation of a critical nucleus based on the Classical Nucleation Theory. (Sloan Jr & Koh, 2007)

This can be interpreted by the excess Gibbs free energy ΔG between the solute in the solution and a small solid particle of solute. This ΔG will be equal to the sum of the surface excess free

energy ΔG_s, plus the volume excess free energy ΔG_V. This can be expressed as: (Sloan Jr & Koh, 2007)

$$\Delta G = \Delta G_s + \Delta G_V = 4\pi r^3\sigma + \frac{4}{3}\pi r^3 \Delta g_V \quad (3)$$

Where:

Δg_V = free energy change per unit volume

σ = surface tension of the interface between liquid and crystal

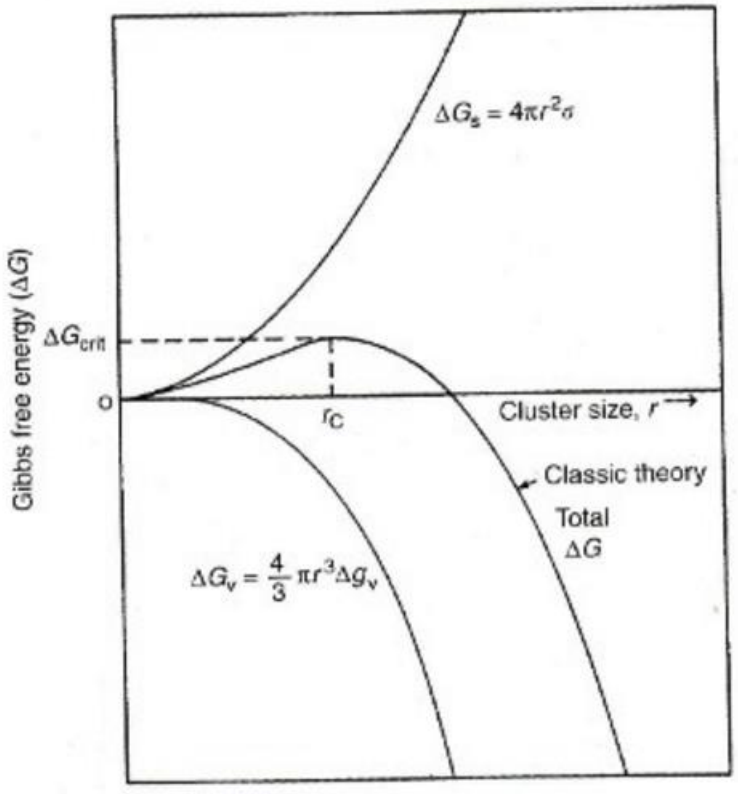

Figure 5: Illustration of volume excess free energy (ΔG_V) and surface excess free energy (ΔG_s) as a function of cluster size. (Sloan Jr & Koh, 2007)

As can be seen on the illustration above, the negative Δg_V causes ΔG_s and ΔG_V to be of opposite sign while being different functions of the same variable, namely the radius of the solid particle r. When adding the two effects together, a maximum value, $\Delta G_{crit,}$ is obtained,

as illustrated on figure (5). This value corresponds to the critical nucleus, r_c. In other words, this point needs to be surpassed before a spontaneous nuclei or cluster grow can be possible. The maximum value of ΔG can be found if by differentiating equation (3) and then setting the result to be zero: (Sloan Jr & Koh, 2007)

$$r_c = -\frac{2\sigma}{\Delta g_V} \tag{4}$$

And

$$\Delta G_{crit} = 4\,\pi\,\sigma\,\frac{r_c^2}{3} \tag{5}$$

The rate that these critical sized clusters are formed is highly sensitive to the value of the free energy barrier (ΔG), or equivalent to how far into the metastable region it is. As the critical cluster size required becomes smaller, so does the amount of free energy barrier that must be overcome to form the critical clusters. Eventually, the barrier is so small that the nucleation process becomes spontaneous. Englezos et al. (Englezos, Kalogerakis, Dholabhai, & Bishnoi, 1987) found an expression to determine the radius of the hydrate critical nucleus using the Gibbs free energy per unit of volume of hydrate formed (Δg_V) by using a modification of equation (4) and (5). This will be explained in more detail in the model analysis section.

2.10. Heterogeneous Nucleation (HEN)

Heterogeneous nucleation, shortened to HEN, is by far the most common occurrence when it comes to hydrate nucleation. If looked at it from an energy point of view, the the nucleation process is usually happening on a two-dimensional surface, for instance on a pipe wall or on a particle, and not on a three-dimensional surface such as free volume of water. The contact angle (θ) between the surface and the hydrate crystal is related to φ, which is a fraction multiplied by ΔG_{crit} for HON in order to give a smaller $\Delta G'_{crit}$ value for HEN: (Sloan Jr & Koh, 2007)

$$\Delta G'_{crit} = \varphi\,\Delta G_{crit} \tag{6}$$

$$\varphi = [(2 + \cos\theta)(1 - \cos\theta)^2]/\,4 \qquad (7)$$

If the contact angle θ is equal to 180˚, i.e. complete nowetting of the substrate, then $\Delta G'_{crit}$ is the exact same as ΔG_{crit}. If θ = 0˚, i.e. complete wetting of the substrate, then $\Delta G'_{crit} = 0$.

It is also worth noting that a foreign surface will effectively lower the value of $\Delta G'_{crit}$ and critical radius (r_c) that is required for spontaneous hydrate growth, as can be seen in equations (6) and (7). Homogeneous nucleation of hydrates departure from this, which is why heterogeneous nucleation occurs a lot more frequently. (Sloan Jr & Koh, 2007)

In 2002, Kashchiev and Firoozabadi (Kashchiev & Firoozabadi, 2002) worked on analysing the kinetics of hydrate nucleation of a one-component gas hydrates in an aqueous solution. They managed to derive an expression for the stationary rate of hydrate nucleation, J, for heterogeneous nucleation at the interface between the gas and the solution or on solid substrates. They also did this for the special case of HON. Their work is based on classical nucleation theory and provides a detailed examination of the mechanisms and kinetic expressions of hydrate nucleation. The classical theory of nucleation can be used in order to determine the work, W(J), that is required to form a hydrate cluster of n building units:

$$W(n) = -n\,\Delta\mu + C\,v_h^{2/3}\,\sigma_{ef} n^{2/3} \qquad (8)$$

Where Δμ is the supersaturation. This represent the work that is gained through the mounting of n hydrate building units that goes into an n-sized hydrate cluster. Nucleation can only happen when then value of Δμ is higher than zero. C is the shape factor. In HON, this shape is a spherical one, and C is then equal to $(36\pi)^{1/3}/3$. In HEN, the shape is a cap cluster on top of a substrate surface, while a lens-shaped cluster is formed at the interface between the gas and solution phases. All this is illustrated on figure (6) below. v_h is the volume of hydrate building units, measured in cubic meters, and is made up of one molecule of gas and n_w (hydration number) water molecules. σ_{ef} is the effective specific surface energy, measured in Joule per square meters, and is the work done to make the interface between the solution and the cluster in HON, or the solution and the substrate in HEN, or solution and gas, also in HEN. (Sloan Jr & Koh, 2007)

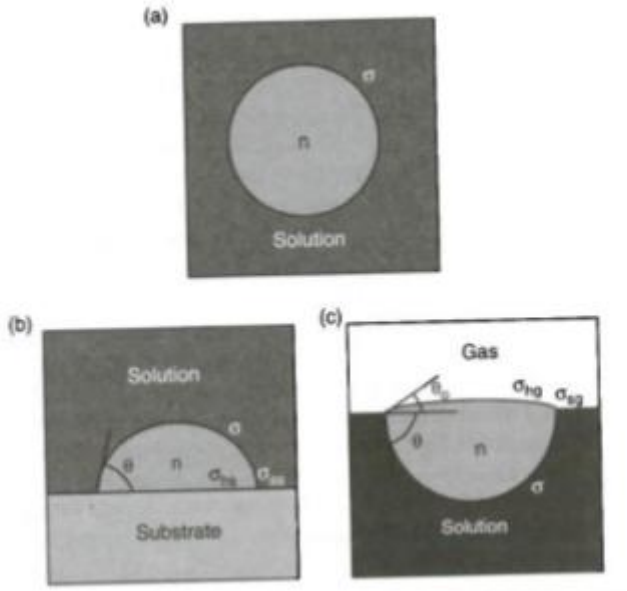

Figure 6: Illustration of (a) is a spherical cluster of n building units in HON, (b) shows a cap-shaped cluster of n building units in 3D HEN on a substrate and (c) which is a lens-shaped cluster of n building units in 3D HEN at the interface between gas and solution. (Sloan Jr & Koh, 2007)

2.11. The Boundary Layer

All of the modern models used today to describe hydrate crystal growth rate include a mass transfer from the bulk phase to the hydrate. What makes this a bit confusing is the fact that often two interfaces are considered, and the driving forces behind the reaction may seem a bit intuitive. (Sloan Jr & Koh, 2007)

The diffusional boundary theory has been well established, with the first concept for an "unstirred" boundary layer being introduced as early as in 1897 by Noyes and Whitney (Noyes & Whitney, 1897). They proposed the simple model:

$$\frac{dm}{dt} = k_d A(c - c^{eq}) \tag{9}$$

Where

dm/dt = rate of crystal growth

k_d = coefficient of mass transfer

A = crystal surface area

c = solution concentration in supersaturated solution

c^{eq} = solution concentration at equilibrium

In the classical work, the importance of k_d is stressed, and set as equal to (D/δ), where D represent the solute coefficient of diffusion, and δ is the thickness of a stagnant boundary layer that is adjacent to the crystal. (Sloan Jr & Koh, 2007)

By the use of interferometry, physical evidence of the existence of such a layer was established, and then the concept was modified to include two steps, namely: (1) diffusion to the interface and (2) reaction at the interface. The first step was a represented my modifying the driving force of the equation, i.e. the $(c - c^{eq})$ term. This was changed to c_i, which is the solute concentration at the crystal-solution interface: (Sloan Jr & Koh, 2007)

$$\frac{dm}{dt} = k_d A(c - c_i) \tag{10}$$

The second step, reaction at the interface, was due to incorporation of the substance into the crystal at the interface:

$$\frac{dm}{dt} = k_r A(c_i - c^{eq}) \tag{11}$$

Where k_r represent a rate constant for the surface reaction.

In this model there is a stagnant boundary layer that is located on the fluid side of the crystal interface, as can be seen on figure (**7**) below. Across this layer there is a concentration gradient which is taken as the bulk fluid concentration (c), and then the interfacial concentration (c_i) in the fluid is subtracted from this. There is however a problem, the interfacial concentration is very difficult to measure accurately, so in order to get around this, the equation is altered by combining equations (10) and (11): (Sloan Jr & Koh, 2007)

$$\frac{dm}{dt} = K' A(c - c^{eq}) \tag{12}$$

Where c_i is eliminated and K' is the overall transfer coefficient, and can be expressed as:

$$\frac{1}{K'} = \frac{1}{k_d} + \frac{1}{k_r} \tag{13}$$

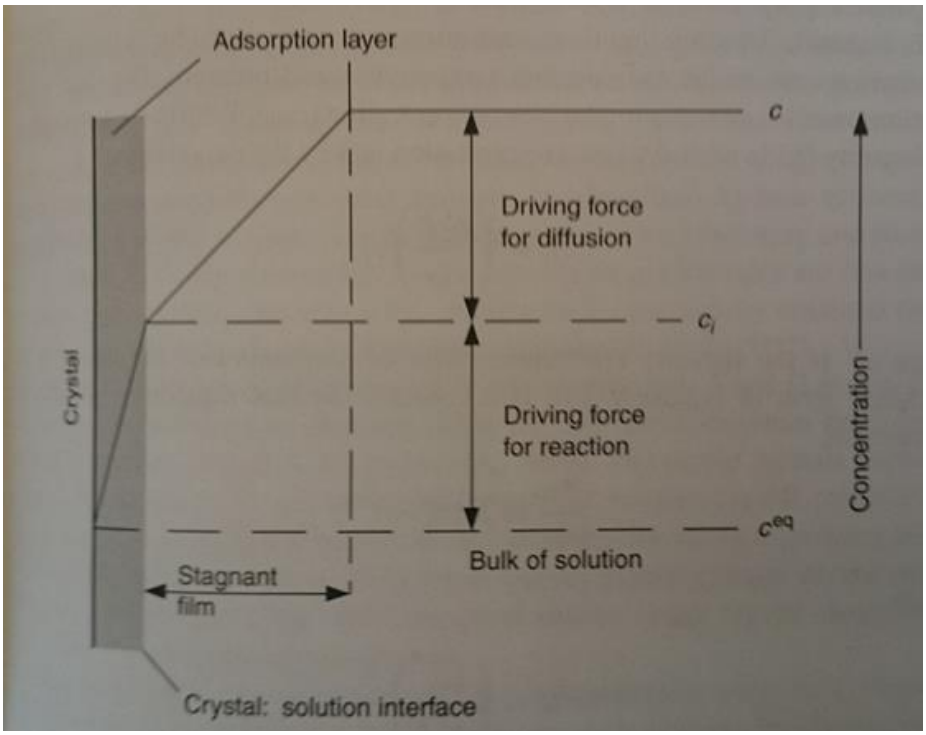

Figure 7: A conceptual model of the mass transfer from the bulk phase to the hydrate.

All of these equations are all different forms of the classical engineering expression which is:

$$Rate = \frac{Driving\ force}{Resistance} \tag{14}$$

Where the difference in concentrations is the driving force. The overall resistance, or 1/K', can be controlled by a low value of either of the two individual coefficients. The crystallisation is mainly controlled by the reaction coefficient (k_r) when diffusion is more rapid, and mass transfer coefficient (k_d) when the reaction is very rapid compared to the diffusion. In any case, the K' value can be approximated based on the value of these smaller k values, while the concentrations in the driving force can be measured (c), or calculated (c^{eq}), instead of non-measureable such as (c_i).

In the modern models surround hydrate growth kinetics, three modifications are often made:

1. The growth rate of the crystal (dm/dt) is instead replaced by the gas consumption rate (dn/dt).
2. The concentrations (c) are replaced by fugacities.
3. The controlling process is sometimes not considered to be either reactor or diffusion through the liquid-crystal boundary layer, but instead diffusion through the boundary

layer at the interface between gas and liquid. An example of this is the Skovborg-Rasmussen model.

When gas consumption is used as the measurement of hydrate growth rate, a pseudo-steady-state approximation is made: at any given time, the rate of gas consumption by the hydrate is equal to the rate of gas consumption from the gas phase. Often times, experiments around this will measure the amount of gas needed to maintain a constant pressure in the gas phase during the formation of hydrate, as to keep the driving force of the reaction constant. In cases like this, the gas consumed from a separate supply reservoir is measured.

2.12. Crystal Growth Process

The crystal growth process is what comes after the initial nucleation. Different from the nucleation process, which is stochastic and very challenging to predict accurately, the crystal growth phase is a lot easier to predict. This process can be placed into 4 sub-categories, known as:

1. Single crystal growth
2. Hydrate film/shell growth at the interface between water and hydrocarbons
3. Crystal growth with interfacial agitation
4. Growth of metastable phases (Sloan Jr & Koh, 2007)

2.13. Single Crystal Growth

During low driving forces in a solution of water and hydrocarbons, hydrates grow as single crystals. When trying to understand the effects additives have on hydrate crystal growth and morphology, it is often beneficial to investigate this type of growth. There are some types of hydrates that can be easily be manufactured a laboratory by using this process, one example being the single crystal ethylene oxide, or single crystal of tetrahydrofuran, shortened to THF. Both of these can be fully mixed in a water solution, and can be isolated for structural analysis. This stands in contrast to the hydrates, which can be very difficult to isolate. So far, only a few successful single crystals that have originated from natural gas have been obtained. (Sloan Jr & Koh, 2007)

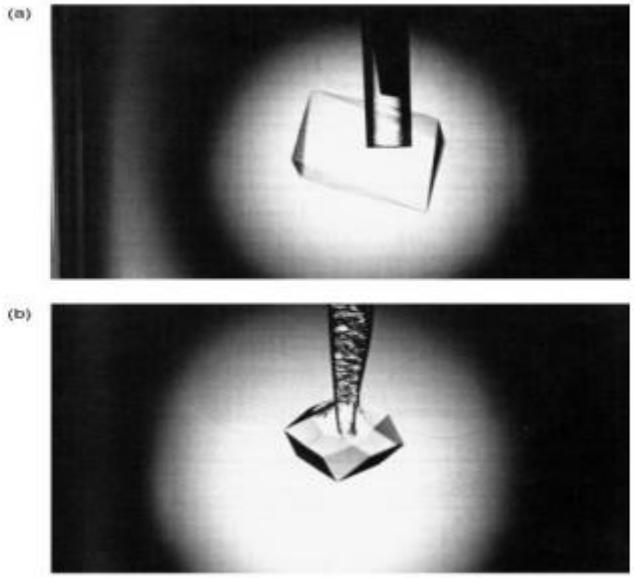

Figure 8: A single hydrate crystal of structure II (a) and structure I (b) (Sloan Jr & Koh, 2007).

An inspection of figure (8) above reveals two instances of isolated crystals, one from structure I (b) and one from structure II (a). The first picture show a single hydrate crystal that has been grown from a stoichiometric solution of THF. The other picture show a single hydrate crystal grown from a stoichiometric solution of ethylene oxide.

2.14. Driving Force of Nucleation

Up over the years a number of different driving forces for nucleation has been proposed. The table below gives an overview of some of these:

Table 1: Different driving forces used for nucleation (Sloan Jr & Koh, 2007)

Investigators	Year	Driving Force
Vysniauskas and Bishnoi	1983	T^{eq} - T^{exp}
Skovborg and Rasmussen	1992	$\mu_{WH}^{exp} - \mu_{WL}^{exp}$
Natarajan et al.	1994	$f_i^{exp}/f_i^{eq} - 1$
Christiansen and Sloan	1995	Δg^{exp}
Kashchiev and Firoozabadi	2002	$\Delta\mu$, supersaturation
Anklam and Firoozabadi	2004	Δg
Arjmandi et al.	2005	T^{eq} - T^{exp}

In most of these cases there has been given little to no justification for the driving forces, based upon equilibrium or nonequilibrium thermodynamics. In this section, a brief justification for a general nucleation driving force will be presented, and to illustrate that the other driving forces are special cases of the more general one. The key component in a hydrate nucleation correlation is the driving force. In essence, the general case driving force is shown below to incorporate all the driving forces mentioned in table 1, although the term ln (f_i^{exp}/f_i^{eq}) dominates (f_i^{exp} and f_i^{eq} means fugacity of a component i at experimental and equilibrium pressure). The subcooling driving force is shown to be the isobaric equivalent of the isothermal general case driving force. (Sloan Jr & Koh, 2007)

The total molar change in Gibbs free energy of hydrate formation, $\Delta g^{exp,}$ was presented as the driving force by Christiansen and Sloan in 1995 (Christiansen & Sloan Jr, 1995). The driving force that they derived has been shown to be the general case for all driving forces for nucleation presented by previous researchers. While a process is under constraints of constant pressure and temperature, it will move towards the minimum value of Gibbs free energy. Figure (9) seen below shows an isothermal route for calculating such a state variable by forming a simple calculable path between the two end points, which is the products, “pr”, and the reactants, rx, at the operating pressure and temperature. In the system, hydrate is considered the product and the water converted to hydrate are considered as reactants. (Sloan Jr & Koh, 2007)

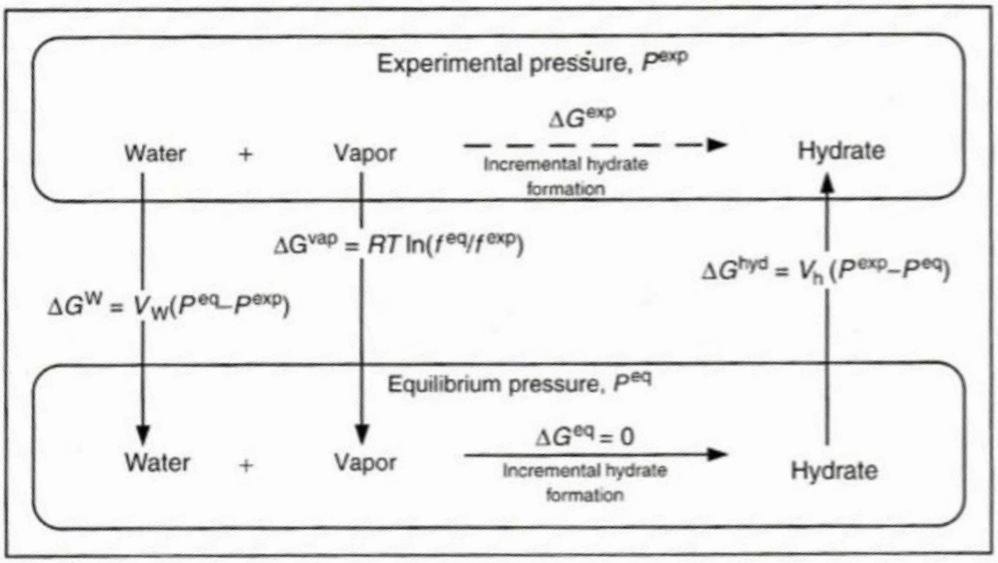

Figure 9: Isothermal path for calculating ΔG for hydrate formation from vapour and water. (Sloan Jr & Koh, 2007)

$$\Delta g^{exp} = \Delta g^{rx} - \Delta g^{pr} \tag{15}$$

Where

$$\Delta g^{rx} = \sum_{i=1}^{N} x_i(\mu_i^{eq} - \mu_i^{exp}) \tag{16}$$

And

$$\Delta g^{pr} = \sum_{i=1}^{N} x_i(\mu_i^{exp} - \mu_i^{eq}) \tag{17}$$

By adding five components of the path, one can determine the difference in molar Gibbs free energy between the end points:

1. Separation of reactants (the gas and liquid) at the experimental pressure of $\Delta g^{sep} = 0$.
2. Lowering the pressure of the two reactants to the equilibrium value.
3. Combining gas and water at equilibrium to hydrate ($\Delta g^{eq} = 0$).
4. Compression of the product hydrate from equilibrium pressure to experimental pressure.
5. Combining hydrate and unreacted water and gas at experimental pressure ($\Delta g^{comb} = 0$).

Only water and gas that react to hydrate are considered in the path above. If the molar Gibbs free enery of (1) the separation, (3) the reaction at equilibrium, and (5) recombination are all taken as zero, then the value of Δg^{exp} would be the sum of step (2) and (4), as shown in equation 8. (Sloan Jr & Koh, 2007)

$$\Delta g^{exp} = \Delta g^{1} + \Delta g^{2} + \Delta g^{3} + \Delta g^{4} + \Delta g^{5} \quad (18)$$

$$\Delta g^{exp} = 0 + \Delta g^{2} + 0 + \Delta g^{4} + 0 \quad (19)$$

Here, Δg^4 is the isothermal compression of hydrate to equilibrium pressure from experimental pressure, where the hydrate is assumed to be incompressible.

$$\mu_H^{exp} - \mu_H^{eq} = v_H(P^{exp} - P^{eq}) \quad (20)$$

In equation (16) and (19) where the reactant water is taken from experimental conditions to equilibrium conditions, Δg^2 is divided into two parts, the first for water, and the second for gas: (1) the water (L) value is similar to that of equation (20), and (2) the gas phase uses a fugacity ratio for each component I: For the water phase which is assumed to be pure water: (Sloan Jr & Koh, 2007)

$$\mu_L^{eq} - \mu_L^{exp} = v_L(P^{eq} - P^{exp}) \quad (21)$$

And for each of the components in the gas phase which can be assumed to contain no water:

$$\mu_i^{exp} - \mu_i^{eq} = RTln(f_i^{eq}/f_i^{exp}) \quad (22)$$

By inserting the equations (20), (21) and (22) into equation (15) one ends up with:

$$\Delta g = v_L(P^{eq} - P^{exp}) + RT\sum x_i ln(f_i^{eq}/f_i^{exp}) + v_H(P^{exp} - P^{eq}) \quad (23)$$

Which is the general case for all driving forces shown in table 1 for exactly 3 reasons:

1. The $(\mu_{WH}^{exp} - \mu_{WL}^{exp})$ driving force presented by Skovborg and Rasmussen is a part of equation (15), which is shown as the leftmost term in equation (20) and (21).

2. For all hydrates, the second term on the right dominates equation (23), and the first and last term is effectively cancelled out, due to the fact that the molar volume of water is within 15% of that of hydrates. The Natarajan et al. driving force which was $(f_i^{exp}/f_i^{eq} - 1)$ is the first term in an infinite series expansion of the second term $(ln(f_i^{exp}/f_i^{eq})$ which can be found in equation (23)-acceptable when (f_i^{exp}/f_i^{eq})< 1.3).
3. The ΔT driving force is a isobaric equivalent to the isothermal Δg in equation (23). The Gibbs-Helmholtz relation can be applied to find:

$$\Delta g = -(s)\Delta T \tag{24}$$

Where the term –(s) is related to the Gibbs free energy term to the change in temperature. (Sloan Jr & Koh, 2007)

2.15. Fugacity

Fugacity is as mentioned used as a driving force for some hydrate growth models, and is therefore worth taking a look into. Essentially, the fugacity is an effective partial pressure of a real gas which basically replaces the mechanical partial pressure when accurately computing the chemical equilibrium constant. For an ideal gas, the fugacity is the same as the pressure, but for real gases the fugacity can be found with the correlation:

$$\varphi = \frac{f}{P} \tag{25}$$

Where

f = fugacity

P = pressure

φ = fugacity coefficient, which is dimensionless

The origin of the whole concept of fugacity comes from the equation:

$$G_i^{ig} = \Gamma_i(T) + RT \ln P \tag{26}$$

Where

G^{ig} = Gibbs free energy

$\Gamma_i(T)$ = integration constant at constant T, and is a species-dependant function of temperature only.

This equation is only valid for pure species I in the ideal-gas state. When it comes to real gases, one must write the equation using the fugacity concept, f_i:

$$G_i^{ig} = \Gamma_i(T) + RT \ln f_i \tag{27}$$

As shown, the fugacity replaces pressure, using the same units, and since equation (26) is a special case of equation (27), and:

$$f_i^{ig} = P \tag{28}$$

Which is the case for an ideal gas, where its fugacity is the same as its pressure. By subtracting equation (26) from equation (27), and write both for the same pressure and temperature:

$$G_i - G_i^{ig} = RT \ln \frac{f_i}{P} \tag{29}$$

The left hand side of this equation is also known as the residual Gibbs energy, or:

$$G_i - G_i^{ig} = G_i^R \tag{30}$$

Which gives the relation:

$$G_i^R = RT\phi_i \tag{31}$$

Which is where the fugacity coefficient comes in. These equations apply to all pure species i in any phase at any condition. Most of the information around fugacity was gathered from the book “Introduction to Chemical Engineering Thermodynamics” 7th edition (Abbott, Smith, & Van Ness, 2001).

3. MODEL ANALYSIS

In this section the focus will be on the approach used by the different authors to end up with their respective models. The different parameters used for the Englezos and Skovborg and Rasmussen models will then be calculated when possible, and when not, available data from similar experiments will be used instead. This will then be used to estimate gas hydrate growth for the experiments conducted in the lab, and then compared to the actual measured results.

the Englezos–Kalogerakis–Dholabhai–Bishnoi model

The Englezos model is based on experimental hydrate kinetic data that was obtained through measuring of gaseous methane, ethane and under isothermal and isobaric conditions mixtures. They conducted the experiments using a semi-batch tank reactor with stirring. The temperature in the tank were being constantly measured while the pressure were kept constant by being constantly supplied with gas. According to this model, the kinetic hydrate formation has a three-step growth process (Skovborg & Rasmussen, 1994):

1. *"Transport of the gas from the bulk of the gas phase to the liquid bulk phase.*
2. *Diffusion of gas from the bulk of the water phase and liquid film to the hydrate crystal-liquid interface through a laminar diffusion layer around the hydrate particle.*
3. *"Reaction" at the interface, which in an adsorption process describes the incorporation of gas molecules into the cavities of the water structure and the subsequent stabilization of the framework of the structured water." (Skovborg & Rasmussen, 1994)*

From this, step two and three are what forms the actual crystallization process. Since there will be no accumulation in the diffusion layer around the particle, the two gas consumption rates must be the same. From that, one can say that the number of gas moles consumed per second per particles will be:

$$(\frac{dn}{dt})_P = K^* \times A_P(f - f_{eq}) \quad (32)$$

Where

$$\frac{1}{K^*} = \frac{1}{k_r} + \frac{1}{k_d} \quad (33)$$

A_p = surface area of particle. These particles are assumed to be spherical, which implies that $A_P = 4\pi r^2$.

f = fugacity of the component in the bulk volume

f_{eq} = equilibrium fugacity of component in the liquid at the interface between gas and water

K * = growth rate of the hydrate. Describes combined rate for adsorption and diffusion.

k_r = the reaction rate constant

k_d = the mass transfer coefficient around the particle

$(f - f_{eq})$ = driving force

To find the global rate at which the reaction occurs, the integral of the rate per particle for all the particles is determined:

$$R_y(t) = \int_0^\infty \left(\frac{dn}{dt}\right)_P \phi(r,t)dr \quad (34)$$

$$R_y(t) = \int_0^\infty K^* \times A_P(f - f_{eq})\phi(r,t)dr \quad (35)$$

$$R_y(t) = 4\pi K^* \mu_2(f - f_{eq}) \quad (36)$$

Where

μ_2 = second moment of the particle size distribution (PSD), which by definition is equal to:

$$\mu_2 = \int_0^\infty r^2 \phi(r,t) dr \tag{37}$$

Here:

r = radius of the particle

t = time

φ(r, t) = crystal size distribution

Because of this, the global reaction rate can be expressed as:

$$R_y(t) = K(f - f_{eq}) \tag{38}$$

Thus, the crystallisation process in the liquid phase is determined using this pseudo-first-order irreversible homogeneous reaction. However, in the actual reactor, the liquid mass is not necessarily homogenous. Because of this, a notional point is introduced. This point is defined as an element of suspension, which is small in comparison to the total contents in the reactor, but just about large enough so that it has an average value of intensive properties, for example the population density and the concentration independent of molecular variations. The logics behind this assumption is that the particle radius, i.e. the radius of the nucleus, are adequately small in comparison to the thickness of the diffusion film for gas absorption. The radius is at least three orders of magnitude smaller than the thickness, which means that one can assume that the reaction is homogenous. Additionally, because of the high agitation, it is assumed that all the hydrate particles are distributed equally in the liquid phase. (Englezos et al., 1987)

The first step in the hydrate formation process is when the gas is transported from the gas phase to the liquid phase. This is described using the two-film theory. Since the partial pressure of the water in the gas phase is very small, gas phase resistance can be neglected. They assumed a quasi-steady-state conditions, which means that the accumulation term in the liquid film can be neglected and therefor the mass balance for gas in a slice of the film with thickness dy and unit cross-sectional area yields: (Englezos et al., 1987; Froment & Bischoff, 1979)

$$D\frac{d^2c}{dy^2} = K(f - f_{eq}) \tag{39}$$

Where

D = diffusivity of the gas

c = concentration of the gas

y = distance from the gas-liquid interface

$K = 4\pi K^{*}\mu_2$.

Since it is possible to write the concentration of the gas in terms of fugacity, while also assuming that the amount of moles of the water remain roughly constant, they got:

$$c = \frac{c_{w0}f}{H} \tag{40}$$

Where

H = Henry's constant (Henry's law)

c_{w0} = initial concentration of water

This means the equation can be written as:

$$D^{*}\frac{d^2Y}{dy^2} = KY \tag{41}$$

Where

$$Y = f - f_{eq} \tag{42}$$

And

$$D^{*} = \frac{Dc_{w0}}{H} \tag{43}$$

By using the following boundary conditions:

$$at\ y = 0: \quad Y = f_g - f_{eq} \tag{44}$$

$$at\ y = y_L: \quad Y = f_b - f_{eq} \tag{45}$$

Here:

y_L = film thickness

f_g = the fugacity of gas in the gas phase

f_b = the fugacity of the gas in the liquid bulk phase

This lead them to the analytical solution of the equation, which is:

$$f = f_{eq} + \left\{(f_g - f_{eq})sinh\left[\gamma\left(1 - \frac{y}{y_L}\right)\right] + (f_b - f_{eq})\sinh\left(\gamma\frac{y}{y_L}\right)\right\}\frac{1}{\sinh\gamma} \tag{46}$$

Where

γ = the Hatta number which is an indication of how quickly the reaction proceeds when compared to the diffusion rate through the film. This number is given by the equation:

$$\gamma = y_L\sqrt{4\pi K^*\mu_2/D^*} \tag{47}$$

The flux at the interface must be determined, which can obtained from:

$$(J)_y = -D\left(\frac{dc}{dy}\right)_{y=0} = -D^*\left(\frac{df}{dy}\right)_{y=0} \tag{48}$$

Then, the rate at which the gas becomes transported to the liquid phase where it is either dissolved or contributes to forming hydrates is related to this flux at the interface by this equation:

$$\frac{dn}{dt} = (J)_{y=0}A_{(g-l)} \tag{49}$$

Where:

$A_{(g-l)}$ = the gas-liquid interfacial area

Combining the equations (46), (48) and (49) into one gives us this expression for the rate of gas “consumption”:

$$\frac{dn}{dt} = \frac{D^* \gamma A_{(g-l)}}{y_L} \frac{(f_g - f_{eq}) \cosh \gamma - (f_b - f_{eq})}{\sinh \gamma} \quad (50)$$

In order to determine the initial conditions for this equation, they needed to measure the number of moles of gas that have already been dissolved into the liquid phase at the turbidity point for each experiment. Now, in order to find the value of the fugacity of the gas in the liquid bulk phase as a function of time, a mass balance in the bulk is made:

$$\frac{dc_b}{dt} = -D * a \left(\frac{df}{dy}\right)_{y=y_L} - 4\pi K^* \mu_2 (f_b - f_{eq}) \quad (51)$$

Here:

a = interfacial area

When this is combined with equation (46):

$$\frac{df_b}{dt} = \frac{HD^* \gamma a}{c_{w0} y_L \sinh \gamma} \left[(f_g - f_{eq}) - (f_b - f_{eq}) \cosh \gamma\right] - \frac{4\pi K^* \mu_2 H (f_b - f_{eq})}{c_{w0}} \quad (52)$$

At the turbidity point, $f_b = f_{eq}$ (minimum fugacity for the hydrate to exist). Here it is implied that the excess gas beyond the three-phase equilibrium concentration is consumed right away to form the hydrate nuclei. (Englezos et al., 1987)

With the mass balance in place, they needed to determine a population balance in order to predict the value of μ_2 vs. time. The population balance used is coming from Kane et al. (1974) (Kane, Evans, Brian, & Sarofim, 1974), and is given by:

$$\frac{\partial \phi}{\partial t} + \frac{\partial (G\theta)}{\partial r} = \theta \psi(r) \quad (53)$$

Where the first term represent the change in number of crystals in the size range r to r + dr vs. time. The second term represent the number of crystals growing into the size range minus the ones growing out of it. The final term indicates the amount of new crystals that nucleated into the size range due to secondary nucleation. Here it is assumed that:

1. The linear growth rate is independent of the size of the crystal;
2. New crystals can be nucleated at time near zero; and

3. The rate of the secondary nucleation is proportional to the second moment of the particle size distribution, that is: (Englezos et al., 1987)

$$\theta = \alpha_2 \int_0^{\infty} r^2 \phi(r) dr = \alpha_2 \mu_2 \tag{54}$$

Here it is implied that the nucleation rate is in fact proportional with the total surface area of the particles. This means, under current assumptions, that it is not necessarily required to solve the population balance equation in order to find μ_2 vs. time. Instead, they solved the following three ordinary differential equations:

$$\frac{d\mu_0}{dt} = \alpha_2 \mu_2, \quad \mu_0(0) = \mu_0^0 \tag{55}$$

$$\frac{d\mu_1}{dt} = G\mu_0, \quad \mu_1(0) = \mu_1^0 \tag{56}$$

$$\frac{d\mu_2}{dt} = 2G\mu_1, \quad \mu_2(0) = \mu_2^0 \tag{57}$$

Here, the linear growth rate, G, is a function of distance from the interface and time, but independent of crystal size. The average growth rate can be determined as follows:

$$G_{avg} = \left(\frac{1}{L}\right)\left[\int_0^{y_L} \left(\frac{dr}{dt}\right) dy + \left(\frac{dr}{dt}\right)_b (L - y_L)\right] \tag{58}$$

Where L = distance between bottom of reactor and gas-liquid interface and the linear growth rate, dr/dt, is given by the equation:

$$\frac{dr}{dt} = \frac{K^* M (f - f_{eq})}{\rho} \tag{59}$$

Where

M = molecular weight of hydrate

ρ = density of hydrate

By combing these two equations they ended up with:

$$G_{avg} = \left(\frac{K^* M}{\rho L}\right)\left[y_L \frac{(f_g - f_b - 2f_{eq})(\cosh\gamma - 1)}{\gamma \sinh\gamma} + (L - y_L)(f_b - f_{eq})\right] \quad (60)$$

The dynamic behaviour of the system is described by the differential equations (50), (52), (55), (56) and (57) with their initial conditions. The model only describes the growth phase of the hydration process, which means the induction phase is disregarded, and starting point is set at the nucleation point, or the turbidity point, n_{tb}. This means they needed to know the values of the different parameters for these equations at this point. For the first two equations, (50) and (52), these boundary values have already been determined at the nucleation point. Englezos et al. (Englezos et al., 1987) claims that this point will always have a higher value than the maximum number of moles of gas that can be dissolved in the water phase. What this means is that the water is effectively supersaturated with gas relative to hydrate formation, and as soon as the hydrate formation starts when the first stable nuclei is formed, this excess of gas is instantaneously consumed in order to for hydrate nuclei. This means the following boundary conditions for equation (50) and (52) are:

$$n(t = 0) = n_{tb} \quad (61)$$

$$f_b(t = 0) = f_{eq} \quad (62)$$

Where n_{tb} is established based on measurements while f_b is calculated using, in this case, the model of Munck et al (1988) (Munck, Skjold-Jørgensen, & Rasmussen, 1988).

For determining the boundary conditions for the other equations, (55)-(57) the amount of excess gas above equilibrium is used. Imagine μ_2 as the number of hydrate particles per unit of liquid volume in the water phase. When the nucleation point is reached, and hydrate start to form, this excess gas will be turned into hydrate nuclei, and can that way be calculated using particle radius, molecular weight and density of the hydrate particles:

$$\mu_2(t = 0) = \mu_0^0 = \frac{N_P}{V_L} = \frac{3M(n_{tb} - n_{eq})}{4\pi V_L \rho r_{cr}^3} \quad (63)$$

Where

N_P = initial number of hydrate particles, assumed to be spherical and of the same radius = critical radius, r_{cr}.

V_L = total liquid volume

And so they had the boundary conditions for the first and second moment given by: (Englezos et al., 1987)

$$\mu_1(t=0) = \mu_1^0 = r_{cr}\mu_0^0 \tag{64}$$

$$\mu_2(t=0) = \mu_2^0 = r_{cr}^2\mu_0^0 \tag{65}$$

This critical radius is defined as the smallest radius at which the nuclei will be stable and continue growing instead of dissolving. Here it is worth mentioning that equation (64) and (65) is the corrected forms of the originally presented equations by Englezos et al in 1987. In the original work they used the particle diameter, as opposed to the radius as the characteristic value of the particle size, which is contradictory to what they did in the rest of the model (Ribeiro & Lage, 2008).

In order to pin point the exact critical radius, Englezos el al (Englezos et al., 1987) used the standard nucleation theory by Khamskii (1969) (Khamskiĭ, 1969) and Nyvlt et al. (1985) (Nyvlt, Sohnel, Matuchova, & Broul, 1985) to obtain the following:

$$r_{cr} = -\frac{2\sigma}{\Delta g} \tag{66}$$

Where

σ = interfacial tension between water and hydrate, this is considered to be equal to that of ice in water.

Δg = free energy change per unit volume of the formed hydrate, this is determined from:

$$-\Delta g = \frac{RT}{v_{hyd}}\left(ln\frac{f_b}{f_{eq}} + \frac{n_w v_w (P - P_{eq})}{RT}\right) \tag{67}$$

Where

v_{hyd} = molar volume of hydrate

n_w = number of water molecules per gas molecule in the hydrate

v_w = molar volume of water

f_b = fugacity of the gas in the bulk phase just before the nucleation process occurs.

The limiting factors for this particular model that prevents it from being a universal model is:

1. It is built around the parameter K*, which basically only works for the most simple hydrate forming gases such as methane, ethane and carbon dioxide. These form sI hydrate, and it is therefore not recommended to use this model when dealing with sII or sH hydrates.
2. During calculation of the critical radius, the model neglects the final term in ΔG, i.e. it assumes that the hydrate will stay at equilibrium pressure instead of the system pressure.
3. In real-life situations, intrinsic kinetics play a small role in the formation of hydrates, as of current knowledge (Sloan Jr & Koh, 2007).

α_2 = Empirical parameter needed to be fitted based on experimental data

K* must also be fitted based on experimental data.

Even though the model has some flaws, the Englezos model serves as a starting point for many of the more recent models, and it therefore very much worth investigating.

3.1. Skovborg and Rasmussen model

The Skovborg and Rasmussen model is based upon the Englezos model, but with some modifications. Their model is based on mass transfer, rather than growth kinetics. The main differences between the two models is:

1. The crystallization population was completely removed from the model. This was due to the fact that the secondary nucleation constant was so low, roughly (10^{-3}), which implied that there was no secondary nucleation taking place, and rather all particle had equal size and growth rate.

2. The hydrate formation growth rate constant K* was believably too high. Skovborg and Rasmussen came to this conclusion when they saw the increasing deviation between measured and calculated values as time passed by. They even suggested that the cause of this error might have had something to do with an error in the mass transfer coefficient through the liquid film, k_L, and that this value was incorrect. A small error in the k_L value will lead to a large error value of K*.
3. After the induction time of hydrate growth, i.e. the first stable nucleation appears, the model predicts a linear growth rate. According to (Skovborg & Rasmussen, 1994), this would not be the case since as the growing continued, the formed hydrates would cover the interface between the water and the gas, thus causing the growth rate to decrease and eventually stop if allowed to proceed for a sufficiently long time period. This effect is not accounted for in the Englezos model.
4. Finally, the amount of gas consumption in terms of moles is a very sensitive parameter in the model, which is unfortunate, since it is difficult to determine the exact number for this at the turbidity point. (Skovborg & Rasmussen, 1994)

With all this in mind, Skovborg and Rasmussen proceeded to make a new model, based on mass transfer. The idea here was that hydrate growth process could be calculated using the restrictions on mass transfer of gas through the liquid film at the interface between water and gas. Their resulting model was as follows:

$$\frac{dn}{dt} = k_L A_{GL} C_{w0}(x_{int} - x_b) \tag{68}$$

Where

x_{int} = mole fraction of gas in the water phase at the water-gas interface in equilibrium with the gas phase at system pressure and temperature.

X_b = mole fraction of gas in the bulk water phase at the water-gas interface in equilibrium with the hydrate phase at system pressure and temperature.

C_{w0} = the initial water concentration

A_{GL} = Gas-liquid interface area (from the works of Englezos et. al.)

k_L = the mass transfer coefficient for hydrate forming component, fitted with the aid of experimental data

$(x_{int} - x_b)$ = driving force

Limits of the model:

1. The model is limited due the fact that a very small error in the driving force will lead to large deviations between calculated and measured results, especially when the driving force is small. A 5% error in the estimated values of x_b or x_{int} equals respectively an error of 14% and 20% in the driving force. This could be improved by having better models to predict the driving force. However this could, as stated by (Skovborg & Rasmussen, 1994), be a no easy task, even more so for small driving forces.
2. There were deviations between the interfacial areas ($A_{(g-l)}$) computed for each gas that varied from 30% to 50%. This can indicate that the model has a self-consistency problem (Ribeiro & Lage, 2008).

3.2. The Herri–Pic–Gruy–Cournil model

Herri et al. agreed with Skovberg and Rasmussen when it came to the important role of the gas-liquid interface in the hydrate formation process. However, they claim that the kinetic models for this process has to be based upon the theory of crystallisation, and thus include the population based equation. Since the Englezos model was developed in 1987, there has been an increase in the availability of experimental particle size distributions for hydrates, which made a first appearance at the end of the 1990s (Ribeiro & Lage, 2008). The results of these experiments shows that both the mean diameter and the total particles concentration in the reactor heavily depends on the rate of stirring. Trying to theoretically predict the observed effects, Herri el al. developed a new kinetic model of the hydrate growth process, which was actually based on the model by Jones et al. (1992) for the crystallisation of calcium carbonate in a gas-liquid reactor with a modification (Ribeiro & Lage, 2008).

The reactor is, according to the model, divided into two different regions:

1. *"the interfacial region, with a diminutive thickness, where only primary nucleation takes place due to high supersaturation;*
2. *the liquid bulk, where crystals growth occurs but primary nucleation is also possible, depending upon supersaturation." (Ribeiro & Lage, 2008)*

Two differential equations describes the dynamic behaviour of the systems. The first originates from a mass balance for gas in liquid bulk:

$$\frac{dCb}{dt} = k_L A_{GL}(C_{int} - C_b) - \frac{4\,\pi I \mu 2}{vH(1-\alpha H)} \quad (69)$$

Where the initial condition is $C_b(0) = 0$, which is pure liquid.

α_H = volumetric fraction of hydrate in the two phase solution hydrate mixture.

I = crystal growth rate

k_L = the mass transfer coefficient for hydrate forming component, fitted with the aid of experimental data

A_{GL} = Gas-liquid interface area (from the works of Englezos et. al.)

C_{int} = concentration of gas at interface

C_b = concentration of gas at liquid bulk phase

Experiments were conducted to determine the value of the product of $k_L A_{GL}$ as a fuction of stirring rate. The results he obtained by this he presented in graph. They thought that the diffusion of gas to the liquid bulk to the surface of the particle would be the limiting step, when it came to the crystal growth rate. This led them to the following relation (Ribeiro & Lage, 2008):

$$I = k_b(C_b - C_{eq})v_H \quad (70)$$

In which:

k_b = mass-transfer coefficient from the liquid bulk to the surface of the particle

C_{eq} = equilibrium concentration of dissolved gas in the presence of hydrate

k_b is calculated using the correlation of Armenante and Kirwan (1989) for microparticles in stirred tanks:

$$k_b = 1.2 + 0.06\omega^{0.52} \quad (71)$$

The second differential equation relates to the population balance in terms of hydrate crystals. This is called the population distribution equation, or PDE, and it assumes that the crystal growth rate is independent of the crystal size, and takes into account nucleation, aggregation and breakage. The PBE is as follows:

$$\frac{\partial \phi}{\partial t} + \frac{\partial \phi}{\partial r} = E(r) + Q(r) \tag{72}$$

Where

E(r) = net contribution of birth/death terms due to crystal aggregation

Q(r) = net contribution of birth/death terms due to crystal breakage

Initial condition = ϕ (r, 0) = 0

This equation is only valid in the liquid bulk, which is where the crystal growth happens. The interfacial region is for the most part responsible for nucleation. The nucleation rate is equal to that of the particles flux at critical radius, r = r_c. By assuming an infinitesimal size for the nucleated crystals, the boundary condition for equation (72) is obtained: (Ribeiro & Lage, 2008)

$$I\phi(0,t) = J_{nuc,int} + J_{nuc,b} \tag{73}$$

The authors (Herri, Pic, Gruy, & Cournil, 1999) adopted an exponential expression for the nucleation rate based on their own data for nucleation time. That is, the number of nuclei per unit volume per unit time as a function of supersaturation, which was expressed as the ratio C/C_{eq}. In the liquid bulk phase, since the concentration is independent on position, they wrote: (Ribeiro & Lage, 2008)

$$J_{nuc,b} = k_1 \exp[-\frac{k_2}{\log^2\left(\frac{C_b}{C_{eq}}\right)}] \tag{74}$$

By assuming a linear gas concentration in the stagnant film, the nucleation rate for the gas-liquid interface becomes:

$$J_{nuc,int} = k_1 \zeta \frac{S^*}{V} \int_0^{\zeta} \exp[-\frac{k_2}{\log^2\left(\frac{C_b}{C_{eq}}\right)}]\, dy, \tag{75}$$

$$h(y) = C_{int} + \frac{C_b - C_{int}}{\zeta} y, \tag{76}$$

Where

$$\zeta = \frac{D}{k_L} \tag{77}$$

And the parameters k_1 and k_2 were fitted according to data on mean particle diameter for the first stage of methane hydrate growth under several different stirring rates, were they used a simplified version of equation (72). (Ribeiro & Lage, 2008)

There were some contributions to particles agglomeration in the population balance equation, which was expressed by the general equation by Ramkrishna (Ramkrishna, 2000):

$$E(r) = \frac{1}{2}\int_0^r \lambda(\sim r, r^*)\phi(\sim r)\phi(r^*)\left|\frac{\partial \sim r}{\partial r}\right| dr^* - \phi(r) \times \int_0^\infty \lambda(r, r^*)\phi(r^*)dr^* \tag{78}$$

Where $\lambda(\sim r, r^*)$ represent the frequency of agglomeration between particles of radius ~r and r^* and $|\partial \sim r / \partial r| = [1 - (r^*/r)^3]^{-2/3}$.

Then they derived a simplified version of the model by Boer et al in 1989 (Boer & Hoedemakers, 1989) for turbulent agglomeration where they got an expression for λ without the dependence on the particle radius: (Ribeiro & Lage, 2008)

$$\lambda = \frac{4}{3}\left[\frac{B}{36\pi\eta_L}\left(\frac{\mu_0}{\mu_1}\right)^3\right]^{0.18}\left(\frac{2\rho_L\varepsilon}{15\eta_L}\right)^{0.41}\left(\frac{2\mu_0}{\mu_1}\right)^3 \tag{79}$$

Where:

η_L = liquid viscosity

ε = energy dissipation rate per unit mass of fluid

B = Hamaker constant of methane hydrate in water, the value of this was estimated from the refractive indices of methane hydrate and water.

The authors (Herri et al., 1999) tried to reproduce the experimental trends for temporal evolution of particle mean diameter by incorporating and testing 4 different additional models: (Ribeiro & Lage, 2008)

1. secondary nucleation in the liquid layer around the crystal
2. breakage by attrition leading to new nuclei
3. binary breakage into two equal particles

4. ternary breakage generating a particle with half of the initial mass and two others with identical mass

From the above models, only model 2, breakage by attrition was able to explain the experimental trends, and this phenomenon was modelled by the relation: (Ribeiro & Lage, 2008)

$$Q(r) = k_3 \omega^{k_4} \mu_2 \delta(r) \tag{80}$$

Where k_3 and k_4 are empirical parameters. They gave a value equal to 3×10^{-12} for k_3, but never mentioned a value for k_4.

They used the method of moments (Ramkrishna, 2000) to solve equations (69) and (72) and find their initial and boundary conditions. The initial six moments of the size distribution were considered in the resolution and the following relation was presented in the closure condition: (Ribeiro & Lage, 2008)

$$\mu_j = (\frac{\mu_1}{\mu_0})^{j-5} \mu_5 \text{ for } j \geq 6 \tag{81}$$

For the agglomeration term to be included, they used a pre-determined expression for ϕ(r) to get the equations associated with the first to fifth moments.

In their work, Herri et al. (Herri et al., 1999) didn't exactly present direct comparisons between experimental and calculated result, as in the previous two models. Instead, they were more concerned their models ability to reproduce the experimentally observed trends (Herri et al., 1999) around the effects that different stirring rates had on the total number of and mean diameter of the particles within the reactor. Because of this, direct result comparing between experiment and model prediction have been focused on the first two models analysed. Something impressive about this model is the fact that it correctly represent both the increases in the initial diameter of the crystals, and reductions the initial particles concentration with an increase in ω. Limiting factors were that the temporal evolutions of the mean particle diameter and the total number of particles was only possible to produce for some tested stirring rates. (Ribeiro & Lage, 2008)

4. EXPERIMENTS

All of our experiments were conducted at the University of Stavanger at a science laboratory. Assisting me with the experiments was PhD student Remi-Erempagamo Meindinyo as a tutor, and bachelor student Kristina Kroknes, who assisted in completing experiments to gain more raw data.

For the experiments 50 ml of distilled water and pure methane gas was used. The methane gas used was of scientific purity grade of 5.5, which corresponds to a purity equal to 99.9995%. The experiments were conducted at a fixed pressure of 90 bar, experimental temperatures of 6, 7 and 8˚C, and stirring rates varying from 225 to 800 rpm (rotations per minute)

Table 1: All of the conducted experiments.

225 rpm	350 rpm	425 rpm	500 rpm	575 rpm	650 rpm	700 rpm	800 rpm
6˚C	6˚C	6˚C	6˚C	6˚C, 7˚C, 8˚C	6˚C	6˚C	6˚C, 7˚C, 8˚C

4.1. Experimental Equipment

All of our experiments were done in a cylindrical test cell as shown on figure below. The test cell is made of titanium walls, has an inner volume of 141,4 ml. The cell consist of a cooling cap, cell wall, top lid, temperature sensors, gas supply tubing, bottom lid , o-rings made of rubber, and with a stirrer blade and magnet in the middle. The cell is covered by another set of walls which the cooling water is allowed to flow through. This is used to lower the temperature in the cell to desired temperature, and then to keep it constant. Thermometers are located both at the inlet and outlet of the cooling water, aswell as at point of entrance of the gas. For the sake of simplicity, any heat loss that may have been lost through the top lid of the cell was neglected.

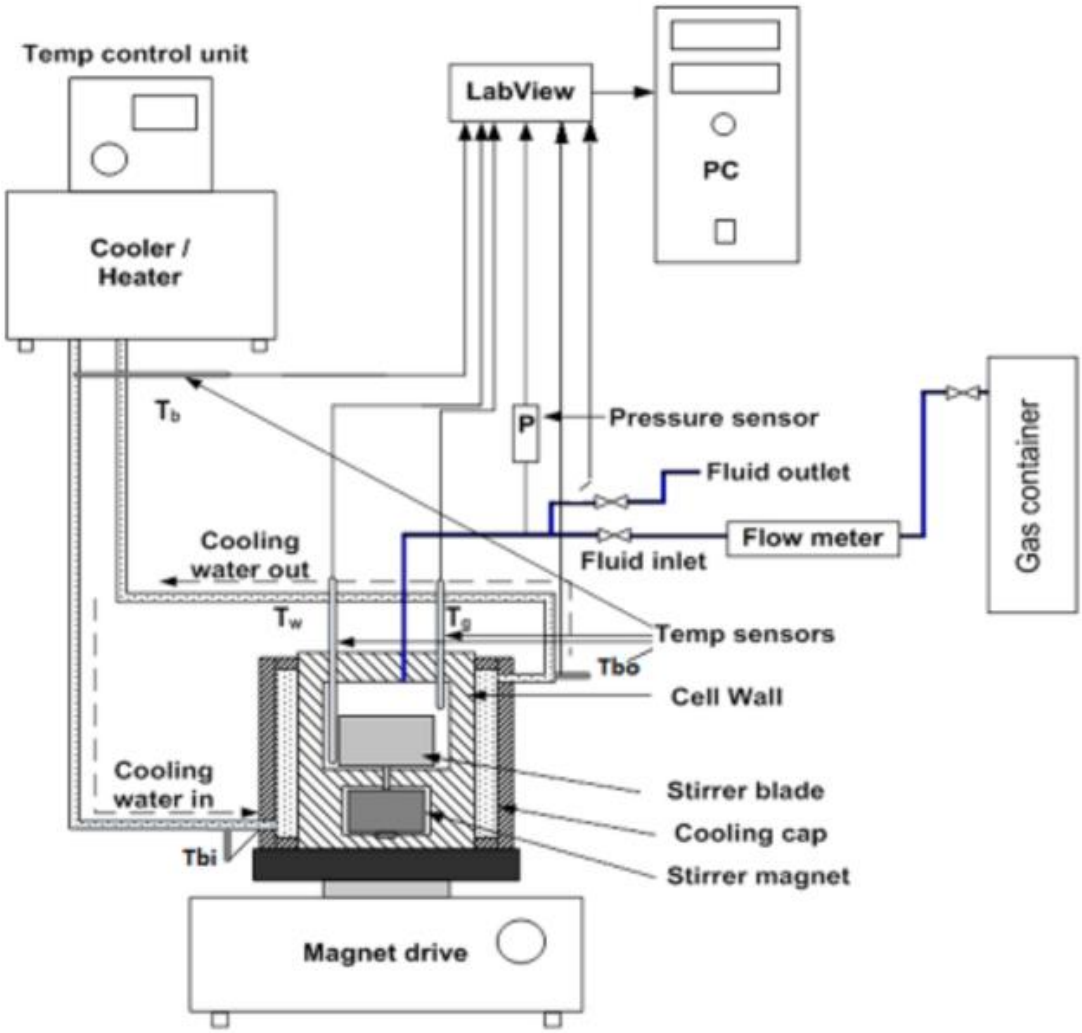

Figure 10: Experimental apparatus. (Meindinyo, Svartaas, Nordbø, & Bøe, 2015)

The temperature control unit used was a Julabo F34, which has a temperature stability of +/- 0.01 ˚C. The pressure sensor was a Rousemount TA3051TA absolute pressure transducer, 0-276 bar absolute, with an accuracy of +/- 0,025 bar up to 100 bar, and after that 0,025% of the full scale. The temperature probes were Pt-100 with an accuracy of 1/10 DIN (+/- 0.03 ˚C at the freezing point of water).

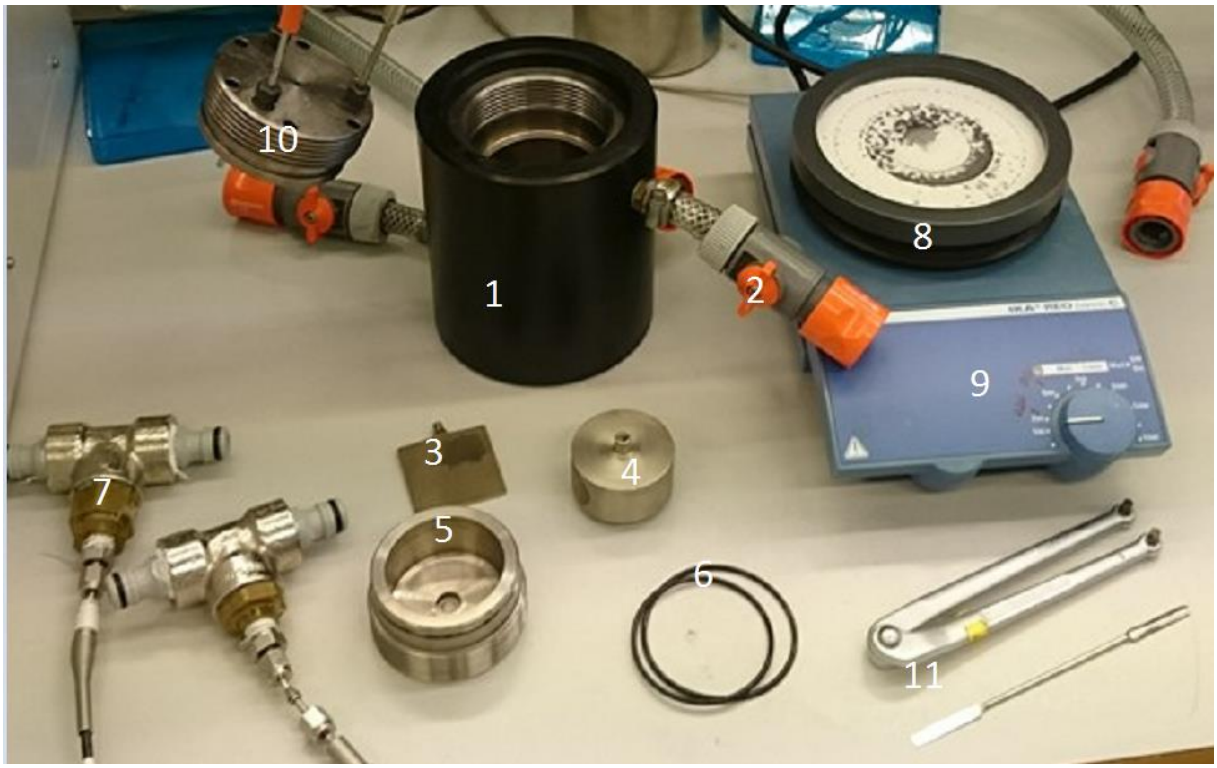

Figure 11: Dismantled experimental cell.

On the figure above:

1. Cooling cap
2. Connections to the cooling bath
3. Stirrer blade
4. Stirrer magnet
5. Bottom lid
6. O-rings
7. Temperature sensors
8. Slot where cell is placed
9. Magnet drive, used to adjust rate of stirring
10. Top lid
11. Tools used to open and close cell.

4.2. Cell Assembly

Whenever I assembled the cell before every experiment, the following procedure was what I used:

1. The Stirrer magnet and blade were screwed together, the magnet placed below the cell and the blade inside it, connected by a hole in the middle.
2. The O-rings was then attached to both the top lid and bottom lid
3. I then filled the bottom lid of the cell with distilled water, roughly 1/5 of the volume. This water is used to squeeze out any unwanted air that could potentially get trapped in the cell.
4. This bottom lid was then screwed onto the bottom part of the cell, causing the water to enter the inside of the upper cell. This water was then emptied into the sink.
5. The Cell is placed on the magnet drive.
6. The main chamber of the cell is loaded with the experimental volume of distilled water, in my case 50 ml.
7. The top lid is screwed into the cell
8. Connect the cell to the cooling bath
9. Gas supply tubing were attached and screwed onto the gas supply, and checked for leakage once pressurised.

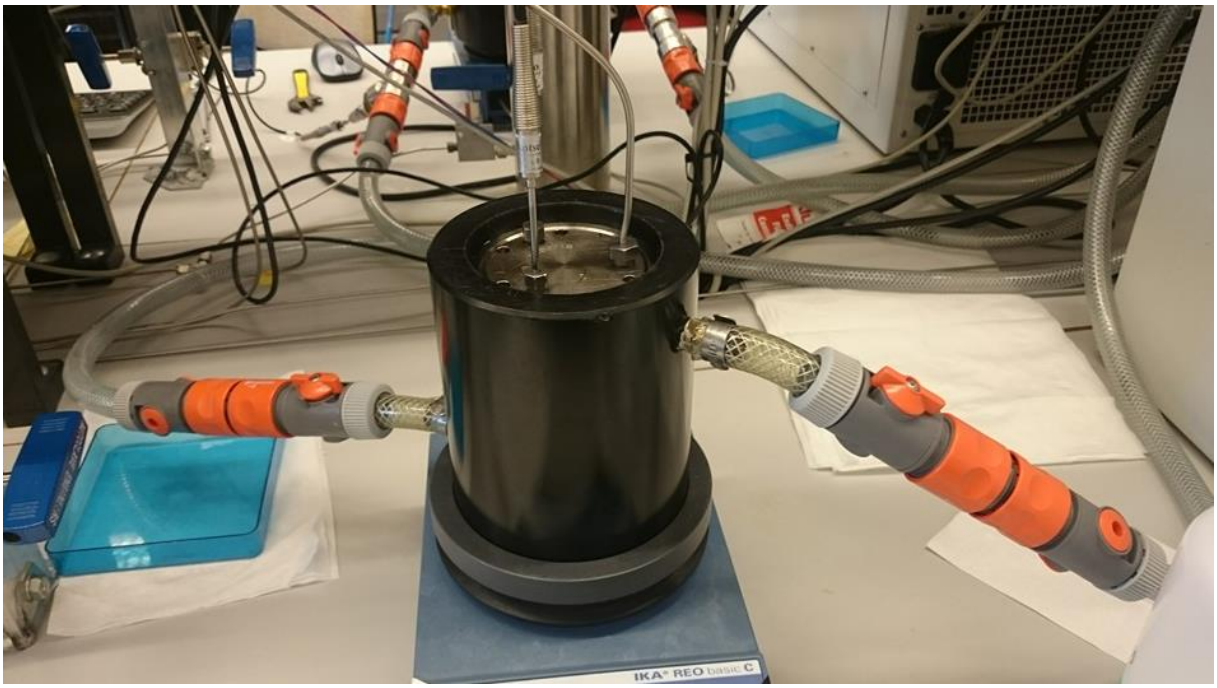

Figure 12: Assembled experimental cell on top of the magnet drive

4.3. The Cooling bath

The cooling bath was used to control the temperature in the experimental cell. It is connected to the cell as shown on figure (10) and (12) with a circulatory system. The bath can be programmed to follow a desired set of commands in terms of the cooling program. It can have up to 60 regulation steps per regulation loop, which can be repeated up to 6 times, before ending the program.

Figure 13: The Julabo F34 cooling bath used.

4.4. Gas container, pressure and boosting

While running an experiment it is paramount that the pressure remains at 90 bar until its completion. In order to ensure this, a gas booster called Resato DBS-160-30-115-D/FUI was used to restore the pressure to 200 bars in the gas container used to supply gas during the experiment. The booster has a capacity of 800 bar output pressure at an input pressure of at least 17.5 bar from the supply bottle. This gas container can hold up to 2.0 l gas, and assisting to maintain pressure during experiments is a backpressure control valve called YARA CRA-SL 400. This is placed between the cell and the gas container and it keeps the pressure constant during the experiment, with roughly 0.5 bar uncertainty. The gas container is connected to a 50 l YARA tank, which is the tank that provide the gas during pressure boosting. This tank should always be at above 150 bar.

4.5. Gas Flow Meter

To measure the amount of gas consumed during the experiment a gas flow meter was used, model Bronkhorst High-Tech-EL-FLOW Mass flow meter/controller digital. It is located in a capillary tube of stainless steel that have resistance thermometer in it. The gas flow meter can control and measure gas flow between vacuum and 400 bar pressure. It is directly connected to the computer used to run LabView via a communicator (FlowDDE) where the experimental data is stored.

4.6. Software

The most important software that used was the previously mention LabView, developed by National Instruments. The main fuction of the program is to display real time experimental data like pressure, temperature, gas flow, stirring rate, time and power consuption from the experimental cell. This data is then stored into logs which can be viewed and analised in

Microsoft Excel, where tables and graphs can be made to illustra the results. Before the raw data is presented in LabView, it goes through the program FlowDDE (Dynamic Data Exchange server), which makes a connection the digital instruments and the Windows application.

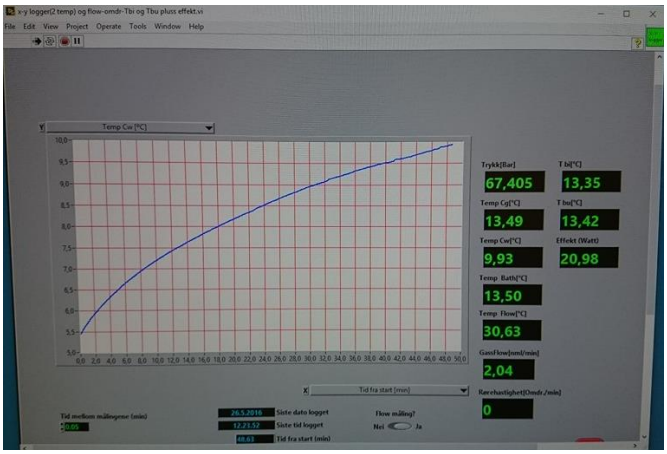

Figure 14: Software LabView used for monitoring and storing of experimental data

4.7. Protective Equipment

Whenever you are working in a lab environment where high pressures and toxic gasses are present, personal safety should always be of concern. During all experimental procedure, specified protective equipment are worn. For this exact experiment, rubber gloves was used to protect from toxins and grease from respectively the cooling bath and the O-rings. In addition, lab coats were used to protect clothing, safety glasses to protect eyes from possible accidents involving high pressure, and hard toe shoes due to the moving of heavy objects, such as the experimental cell itself. While in the process of cleaning and drying the cell, hearing protection was also used due to high noise from the compressed air.

4.8. Cell Cleaning

Before every experiment, all of the equipment which will be used must be cleaned. In order to do this, all the components were disconnected and cleaned first with soap under spring water, and then dry them off using compressed air. Afterwards, everything was cleaned again, this

time using distilled water, and then dried completely again. Once this was done, some grease was applied to the rubber O-rings and cell connections when necessary.

4.9. Cell Filling & Cooling program

When the cell were completely clean, the different parts were connected following the procedure explained under cell assembly. Furthermore, all the air in the cell had to be purged so that it does not interfere with the results. This was accomplished by pressurising the cell up to 40 bars with methane gas, and then bleeding the pressure off using pressure valves. This was done twice to make sure all the air is completely gone before the cell was loaded to the final experimental pressure, which in our case was 90 bar.

Now that the cell is ready, the temperature inside needed to be cooled to the right temperature for the experiment. To do this, a temperature control unit was used to make a program which cooled the cell to given experimental values over a given set of time. To make sure the results were as accurate as possible, it was first instructed to 10 min before starting the cooling, and then only lowered the temperature by 3 ˚C per hour. The initial temperature of the cooling water were 13,5 ˚C, this means that for an experiment ran at 6 ˚C, the corresponding cooling time would be equal to:

$$t = \frac{13{,}5 - 6}{3} \times 60\ \text{min} = 130\ \text{min} \tag{82}$$

After this time, the temperature would remain constant for another 10 minutes, before the stirrer blade would be automatically turned on. This is in order to make sure the actual temperature inside the cell is what should be, since it were usually lagging a bit behind compared to the temperature in the cooling bath. Once the stirring blade starts, the experiment is officially started.

The experiment ran until hydrates formed in the cell, at which point the experiment was ended and warmed back up to initial temperature. Once the hydrates were melted and stirring stopped, the remaining gas in the reactor cell was released. Finally, once the temperature and pressure were back to normal conditions, the cell could be dissembled, and remaining distilled water could be emptied into the sink, and the cleaning process was repeated.

4.10. Dissociation process

Once the experiment is completed, the hydrate within the cell needed to be dissociated, and the pressure lowered so the cell could be safely disconnected and prepared for the next experiment. This was done by first closing the gas supply valve, stopping the stirring and turning the temperature in the cooling bath back up to 13.5 ˚C. Afterwards the pressure could be slowly down to 40 bar, where it is left while the stirring is turned back on and hydrate dissociation process is started. The cell was then left alone for roughly 30 minutes in this state so that the pressure and temperature inside got stabilized. Upon returning, the pressure within the cell would have increased to somewhere between 70 and 90 bar, due to the dissociation and increase in temperature. Next step was to continue to lower the pressure within the cell slowly down to atmospheric pressure. This would accelerate the dissociation process which is endothermic and will therefor lower the temperature in the cell quite significantly. Once temperatures around 13.5 ˚C and atmospheric pressures were reached within the cell, the top lid could safely be removed from the cell, and preparations for the following experiment could begin.

5. DATA ANALYSIS

For every set of experimental condition, in regards to stirring rate and temperature, 3 identical experiments were conducted in order to get an idea of the reliability of the acquired data.

5.1. Before start of hydrate growth

The time between the start of the experiment and the start of hydrate growth is an interesting one, and it can provide information regarding the solubility of methane in water. By looking at the temperature graph, it is possible to identify at what point hydrates first form due to its exothermic properties.

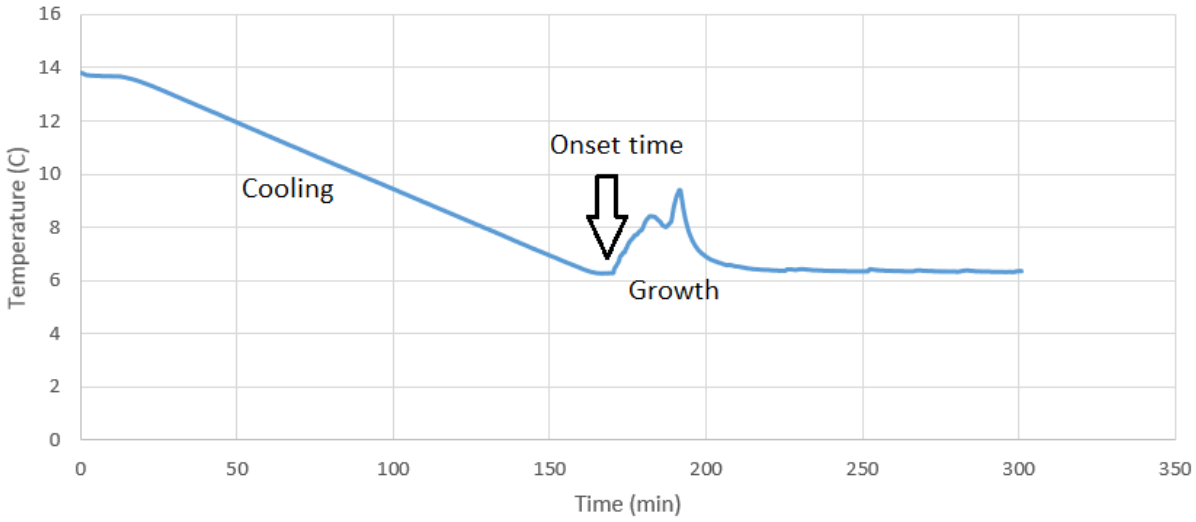

Figure 15: Generic temperature profile for hydrate growth (350 rpm and 6˚C)

As seen on the figure above, a jump in temperature indicate the start of hydrate growth. This can vary from experiment to experiment, even those ran at identical conditions due to the stochastic nature of the nucleation process.

The start of hydrate growth can also be discovered by using pressure data. Below is an illustration of a pressure profile that show a small pressure drop at around the same time as the spike in temperature. This drop in pressure appears due to balancing of the input flow of gas.

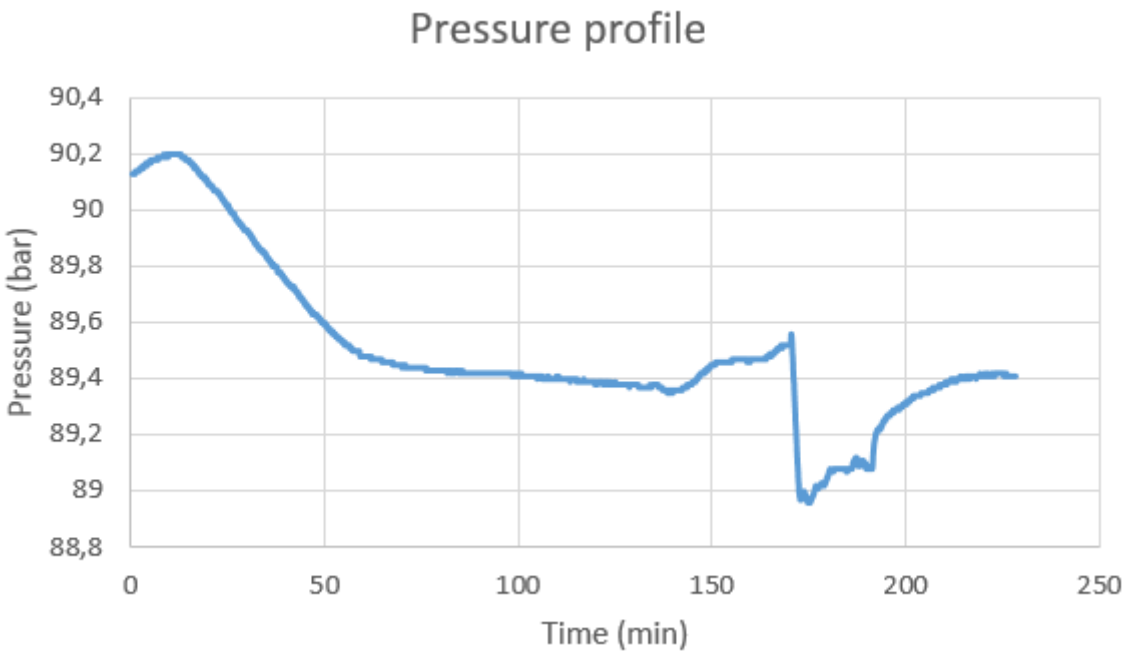

Figure 16: Pressure profile of a 350 rpm 6˚C experimental run.

By measuring the amount of hydrates consumed before any hydrates are formed, one can identify how much methane is dissolved into the 50 ml of distilled water inside the cell, and thus estimate the solubility.

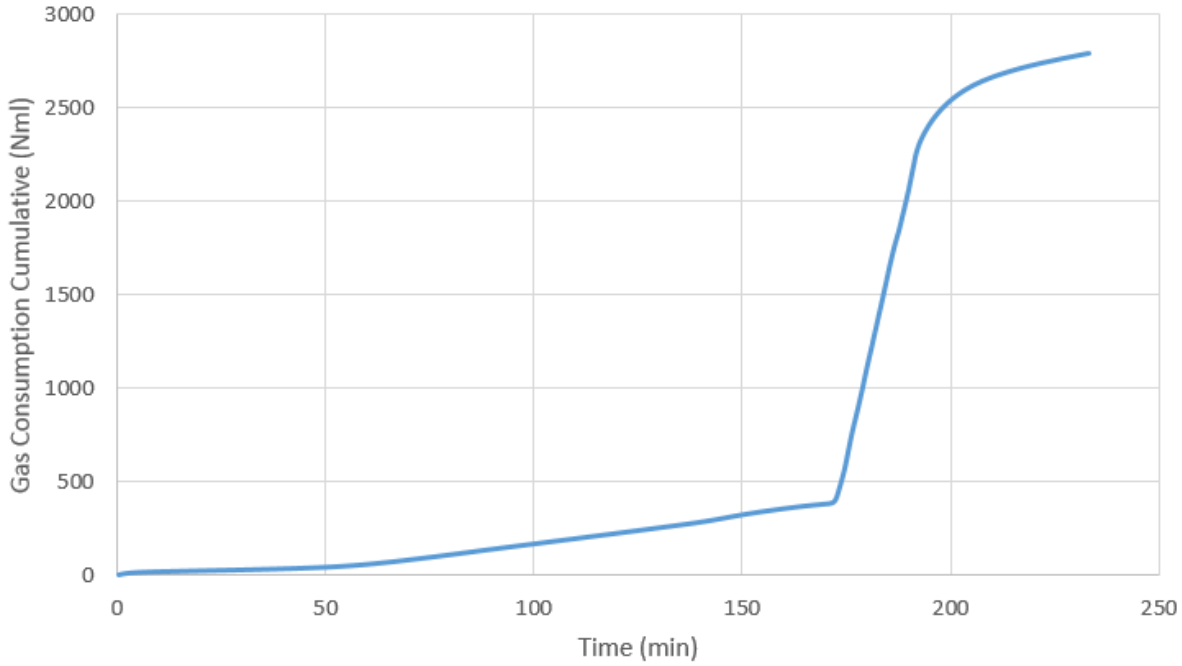

Figure 17: Typical gas consumption profile (350 rpm and 6˚C)

Here, the amount of gas consumed is measured in Normal millilitres (Nml), and the start of hydrate growth can be identified by the acceleration of gas consumption at around 170 min. By using the exact value of gas consumed up until this point one can determine the solubility, after first adjusting for change in pressure and temperature using the gas law:

$$PV = znRT \tag{83}$$

Which becomes:

$$dn = \frac{P_2 V}{zRT_2} - \frac{P_1 V}{zRT_1} \tag{84}$$

Where dn represent change in moles due to mostly cooling, since the pressure is kept close to constant. Right hand side of subtraction sign represent initial conditions, and left hand side represent condition just before hydrate growth.

Now, the only unknown in the gas law is n, or moles, which means it can be calculated and then adjusted with respects to cooling and that way find the actual number of moles dissolved into the water. The solubility is found:

$$Solubility = \frac{actual\ n}{volume\ of\ water} \tag{85}$$

Using this information one can also determine the Henry's number, which plays an integral part in later calculations using the simple formula:

$$Henry's\ Constant = \frac{Pressure}{Solubility} \tag{86}$$

This approach is quite unreliable, since there are some uncertainties in the measuring tools which over a long duration of time can cause quite large deviations in results. Because of this a different approach to identifying solubility and Henry's law constant was used primarily, while this method was used more as an indication to support the credibility of the other method. This will be explained more later.

5.2. Data Reliability

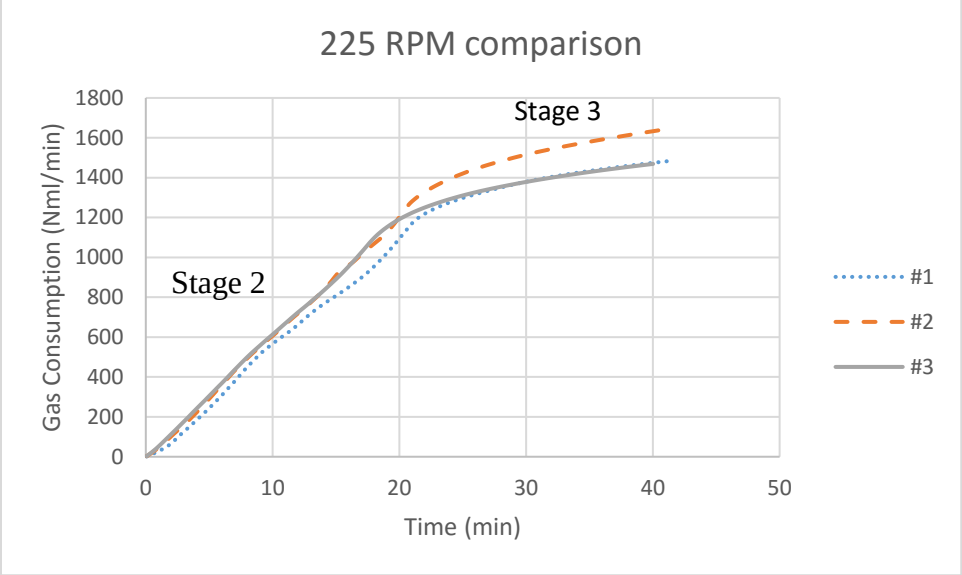

Figure 18: Gas Consumption vs Time at 225

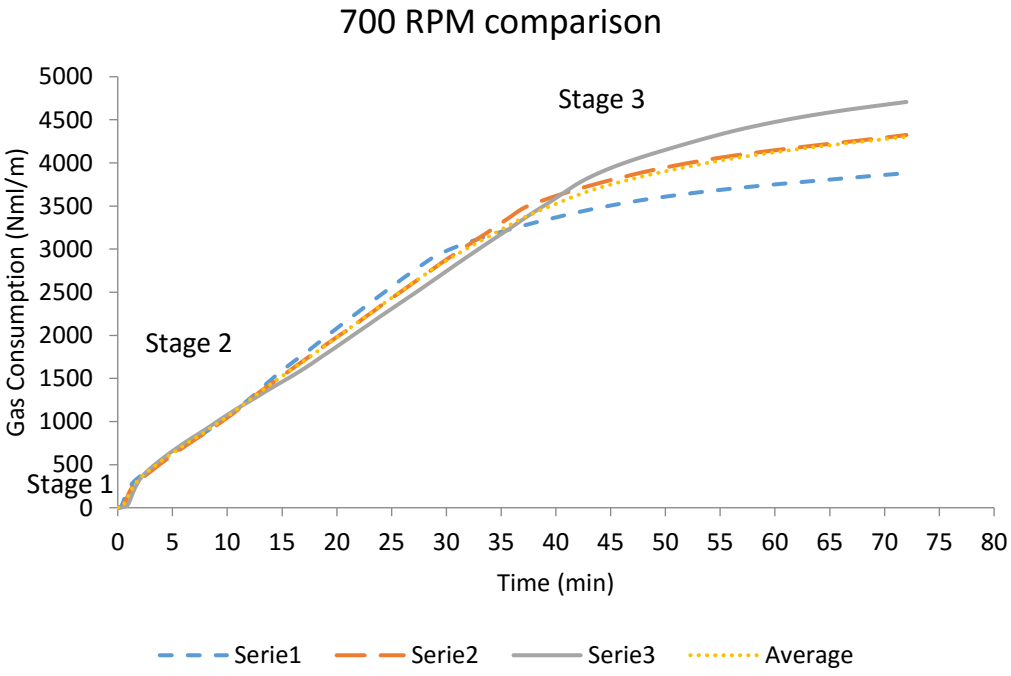

Figure 19: Gas Consumption vs Time at 700 rpm

The figures above shows the gas consumption versus time for two different experiments with 3 identical runs at 225 rpm and 700 rpm for both at 6 ˚C. Ideally the graphs would fall perfectly on top of each other, but as can be seen, they show some variance between the three identical runs. Given the nature of hydrate growth, this is only to be expected.

5.3. *Power Consumption*

During every experiment the power consumption of the stirring blade were measured. Since the blade and the cell is exactly the same between every experiment, the only factors that theoretically should affect the power consumption is then the rate of stirring, and the viscosity of the liquid. Due to this fact one can look at the power consumption profile of an experiment and get an idea of the state of hydrate growth in the cell.

As the cell is filled with more and more hydrate, the power consumption of the stirring blade increases up until a certain point. There are two possible outcomes after this, much dependant on the stirring rate. A lower stirring rate will most likely end up reaching a peak in power consumption before the stirring blade gets stuck in the hydrates filling the cell, which leads means the energy transfer from the stirring to the fluid seizes. If the stirring rate is very high, the stirring blade may end up push all the hydrates aside, which means the stirring may continue with lowered resistance. In our experiments, the first outcome was the most common.

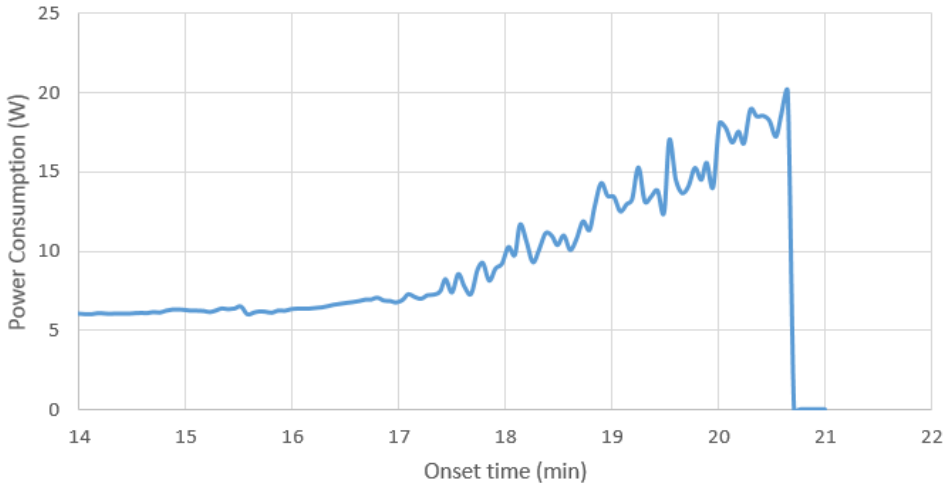

Figure 20: Profile of power consumption versus onset time for a 350 rpm 6˚C experiment.

5.4. *Gas Consumption*

The amount of gas consumed was calculated by the formation of gas hydrates based on the data from the gas flow meters that measure the amount of gas flowing into the cell. Here is the gas consumption rate as a function of time:

$$Gas\ consumption\ rate = \frac{dV_g}{dt} \tag{87}$$

Where

V_g = volume of gas

t = time

By integrating this it is possible to find the cumulative amount of gas consumed:

$$V_g = \int_{t=0}^{t} \left(\frac{dV_g}{dt}\right) \times dt \tag{88}$$

Where t = 0 is the start of hydrate formation, or onset time, and t is the end of the experiment

Since Excel was used for calculations, which doesn't directly support or understand integral, he trapezoidal approach was used instead, which is a good approximation of the actual integral value. The way this approach works is that the area under the graph is split into smaller sections based on time where the height is equal to the average value of the start and end point of each section. These sections are then then summarized in order to find the end value, which is the cumulative gas consumption.

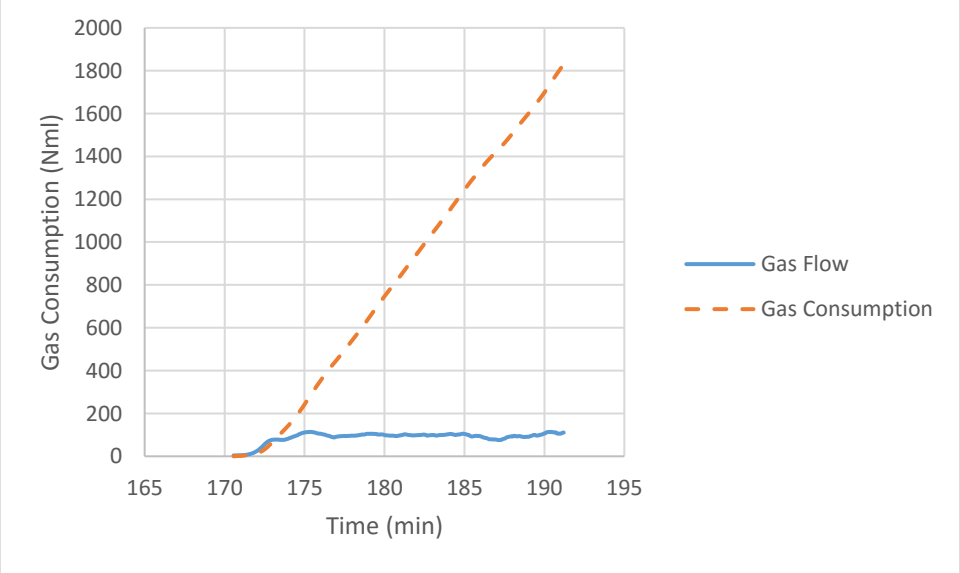

Figure 21: Shows a gas flow and a gas consumption plot for a 350 rpm 6˚C experiment.

5.5. Hydrate growth rate

The hydrate growth rate can be separated into three different stages as to better analyse the data. Stage 1 is where the initial hydrates are formed right after nucleation and the growth rate is very rapid compared to the others. It only lasts for a couple of minutes. This is followed by stage 2 which is longer and have a much more constant growth rate, and is where most of the hydrate growth takes place, even though the growth rate is lower than in the initial phase. Stage 3 is the final phase and now the growth rate is very low and the hydrate growth process is coming to an end. Below is a figure of a temperature profile of a 700 rpm experiment. One can see where the different stages occurs:

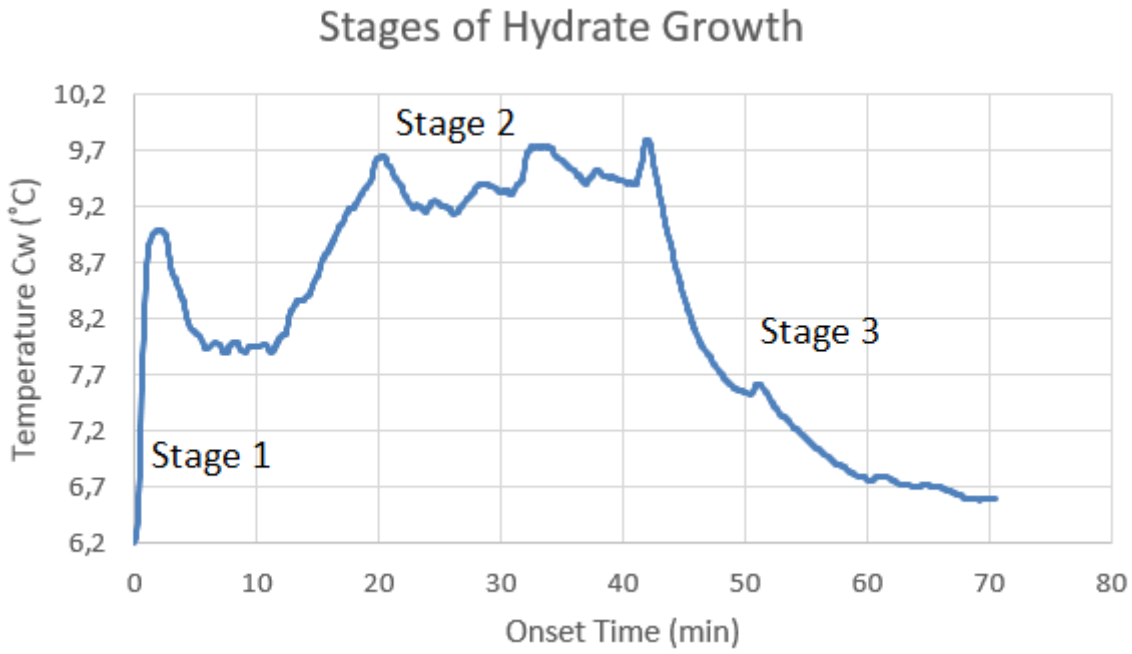

Figure 22: Temperature profile of a 700 rpm 6 ˚C experiment, indicating the three different stages of hydrate growth rate.

One can determine the measured growth rate in the different stages by plotting cumulative gas consumption versus onset time. Using the trendline function in Excel it is possible to get a decent estimation of the growth rate since it is rather constant.

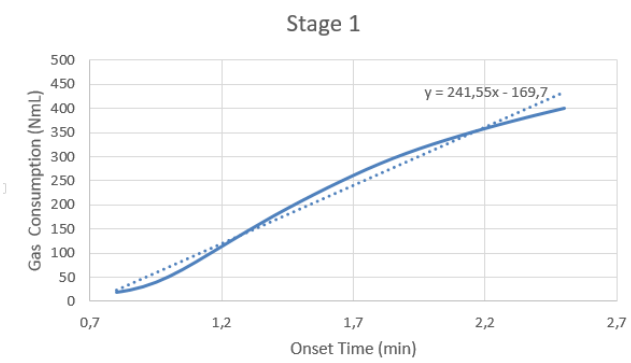

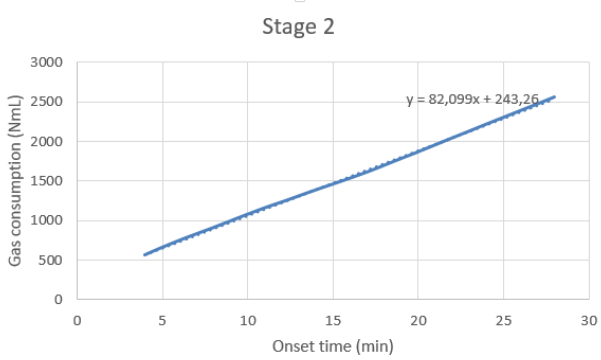

Figure 23: Stage 1 growth rate

Figure 24: Stage 2 growth rate

As seen on the two figures above, the hydrate growth rate follows an almost constant rate, especially so in stage 2. The different growth rates are 241,55 Nml/min and 82,099 Nml for stage 1 and 2 respectively.

5.6. Water to hydrate conversion

As the experiment goes on, more and more of the initial water in the cell will be converted to gas hydrate. This fraction can calculated based on measured data for gas consumption, and initial values. To begin with, the exact number of water molecules present in the cell when the experiment begins must be known. Since the volume and density of water is known, which is 50 ml and 1000 kg/m^3 respectively, and the molar mass of water, which is 18,015 g/mol, the number of moles can be determined as follows:

$$n_w = \frac{V_w \times \rho_w}{M_w} \tag{89}$$

Where

V_w = volume of water

ρ_w = density of water

M_w = molar mass of water

Solving this equation using SI-units, the value of n_w is found to be 2.775 moles. According to Englezos (Englezos et al., 1987), for every 1 mole of methane gas consumed to make hydrates, 5.75 moles of water will also be consumed. Keeping this in mind, one can calculate the fraction of water left in the cell based on cumulative gas consumed:

$$f_w = \frac{n_w - (5.75 \times n_{GC})}{n_w} \quad (90)$$

Where n_{GC} is the amount of gas consumed in moles.

Or, if one wants to know how large fraction of the volume in the cell is hydrates:

$$f_h = 1 - f_w \quad (91)$$

5.7. Turbidity Point

Englezos describes the turbidity point as the point at which the gas consumption rate becomes more or less constant for a certain amount of time. This point is needed for calculations used in the Englezos model where the number of moles consumed by the turbidity point is essential. The reason behind this rather odd initial growth rate is that the liquid is oversaturated with methane just before the start of hydrate growth, which sometimes causes a small burst in growth rate. This point can sometimes be easily determined from a gas consumption plot, while other times it is more challenging, especially for lower stirring rates. If one take a closer look at the second gas consumption plot it the data reliability section, the turbidity point can be determined:

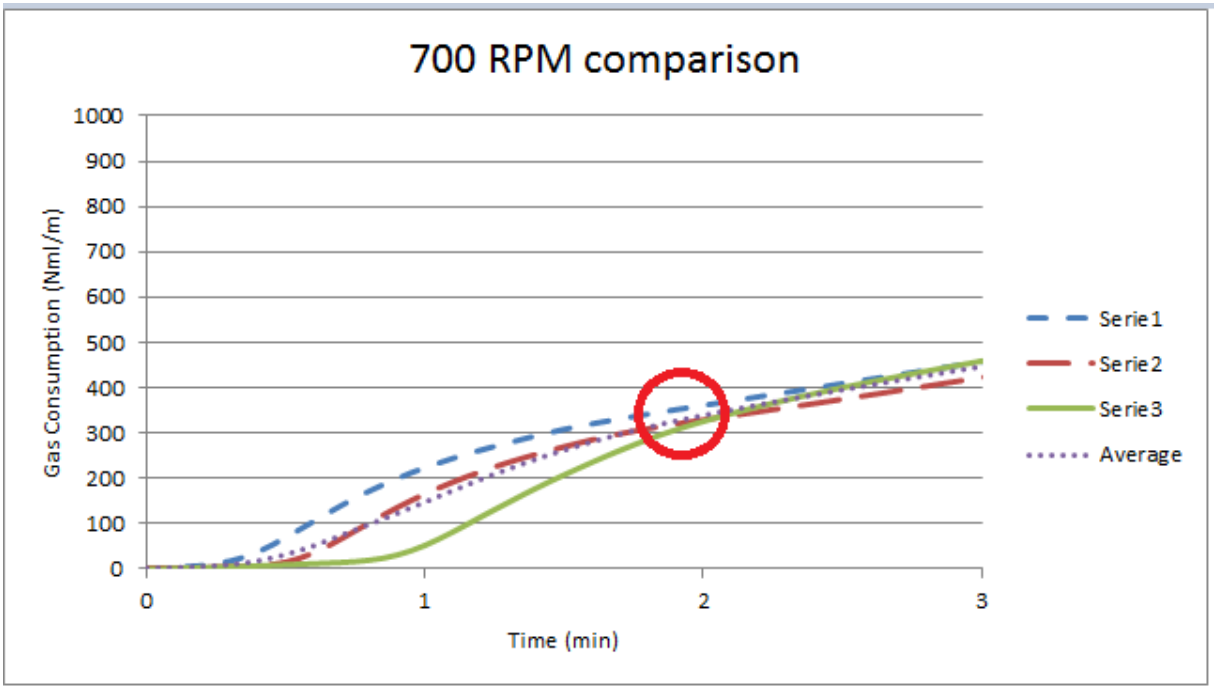

Figure 25: This is a zoomed in look at the 700 rpm 6 ˚C experiments as shown in figure 19**.** The turbidity point is marked by the red circle.

Here the turbidity point can be seen at the 2 minute mark. However, in the other plot, there are no clear indication of this. The reason for this is that the supersaturation state is obtained locally at the interface between gas and water. This becomes a major problem when using the Englezos model to predict the hydrate growth rate, as a small difference in the number of moles consumed at the turbidity point causes large effects on the result. As described in the 1994 paper by Skovborg and Rasmussen, (Skovborg & Rasmussen, 1994) a 5% change in n_{tb} causes an identical change in the result as a 31% change in K*, which is the combined rate parameter. The way around this used in this thesis was to simulate the value of n_{tb} based on experiments where it is apparent, and then use this to make an estimated value for the rest, even though this might have some bad influence on the results in some cases, and must therefore be kept in mind.

6. RESULTS

The bulk of the result data are presented in Appendix B. The data that demanded further explaining or analysis is presented in this section.

6.1. Predetermined parameters

In order to calculate my own prediction for the gas consumption, and then compare these with the experimental result, there are certain parameters which must be determined first. One of these are the volumetric mass transfer coefficient, k_La, which can be used to determine the film thickness. This parameter can be determined by several different approaches, the dynamic physical absorption method presented in the paper "Gas-Liquid Mass Transfer in "Dead-End" Autoclave Reactors" by R. V. Chaudhari and R. V. Gholap et al. (Chaudhari, Gholap, Emig, & Hofmann, 1987) was chosen in this thesis.

The paper presents a method to predict the value of the volumetric mass transfer coefficient based on:

N = speed of agitation

V_g = volume of gas

V_l = volume of liquid

dI = diameter of impeller

dT = diameter of tank

h_1 = height of impeller

h_2 = height of water

The formula is as follows:

$$k_L a = 1{,}48 \times 10^{-3} \times N^{2{,}18} \times \left(\frac{Vg}{Vl}\right)^{1{,}88} \times \left(\frac{dI}{dT}\right)^{2{,}16} \times \left(\frac{h1}{h2}\right)^{1{,}16} \quad (92)$$

Another one is the interfacial area per unit of liquid volume between the liquid and gas, $A_{g\text{-}l}$. At the time of writing this thesis, no means to measure or calculate this in our experiments was available, and data from the works by Englezos was used. Unfortunately, exact dimension of the reactor cell he used is not mentioned in the paper, which makes it almost impossible to know how these data values would changes with regards to stirring rate. Because of this, a constant value of 92.9 cm^2 is used, but this will affect the changes in the kinetic growth parameters with respects to rpm.

Diffusion coefficient was determined using the formula given in the book "Chemical Reaction Engineering and Reactor Technology" by T.O. Salmi, J.P. Mikkola and J.P. Warna (Salmi, Mikkola, & Warna, 2011):

$$D_{AB} = \frac{7{,}4 \times 10^{-12} \sqrt{\phi M_B} \times T}{\mu_B V_A^{0{,}6}} \quad (93)$$

Where

ϕ = association factor for water, equal to 2,6 (Salmi et al., 2011)

M_B = molar mass of methane

μ_B = viscosity of the water

V_A = molar volume of methane, equal to 37,7 cm^3/mol (Salmi et al., 2011).

Surface tension between water and ice is another one that is quite difficult to find an exact value for. According to I.R. Türkmen, 2007 (Türkmen, 2007), this value can be calculated using the formula:

$$\sigma_{i/w} = 28{,}0 + 0{,}25 \times T \quad (94)$$

Where T is temperature in Celsius. However, this formula only applies for temperatures between 0 and - 36 ˚C, and the experiments conducted in this thesis are conducted at positive

temperatures. It is possible that some minor errors can be caused by this, but at the time of writing, no more reliable source was found. Using the model for experimental temperature gives a surface tension between water and ice of roughly: $\sigma_{i/w} = 0{,}03$ J/m^2 (with SI-units).

Second moment of particle size distribution, μ_2, proved to be impossible to calculate based on available data, which was instead determined from data provided by Clarke and Bishnoi (Clarke & Bishnoi, 2005). In their works, a plot is given for second moment of particle size distribution versus time:

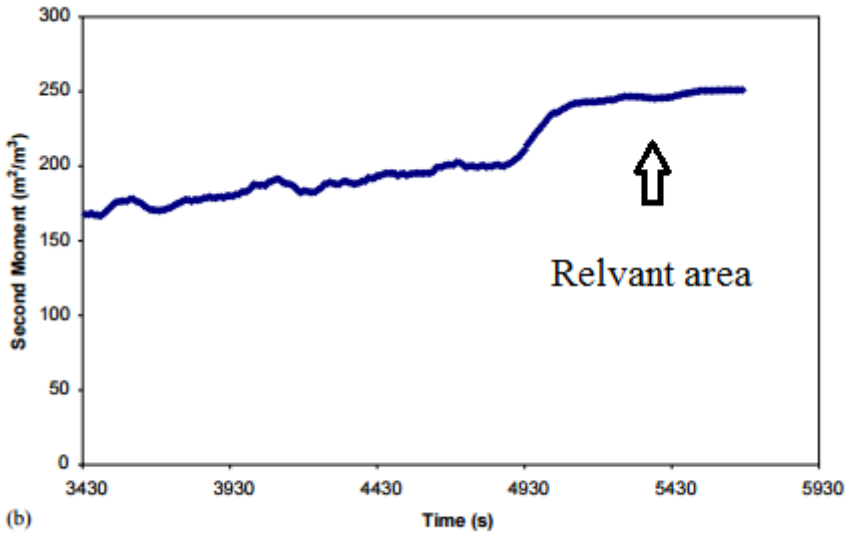

Figure 26: Second moment during hydrate formation at 277.15 K, 21.87 bar and 450 rpm. (Clarke & Bishnoi, 2005)

Yet again, no definitive approach is presented which allows this value to be tabulated to relevant conditions. Nonetheless, the value appears to deviate little during the relevant time, which is hydrate growth stage 2, meaning that even though the initial value used is to some degree incorrect, this can be remedied by K^* which is fitted afterwards.

6.2. Equilibrium Pressure

In order to estimate the equilibrium pressure between the start and end of hydrate growth, a program called CSMGem was used at the university lab to find the exact values at certain temperatures, and then the trendline function in Excel to estimate the values in between.

Temp	PressureEq
6	42,523
7	52,692
8	58,489
9	65
10	72,371

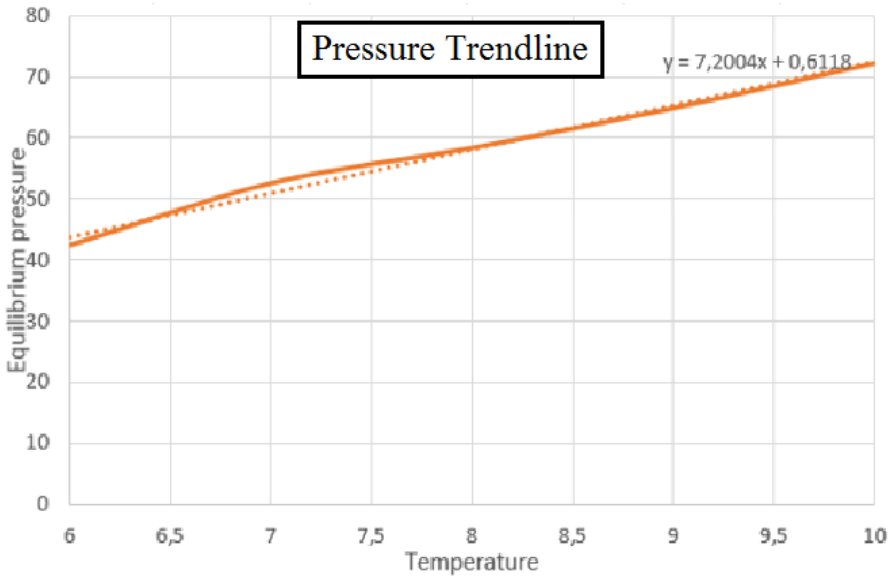

Figure 27: Estimating the equilibrium pressure based on Excel trendline. Table to the left is the exact values from CSMGem.

As seen on the figure above, the equilibrium pressure to the relevant temperature range follows an almost linear line, which is equal to y = 7.2004x + 0.6118. Here, y is the equilibrium pressure and x is the input temperature. This is done in order to find the saturated pressures given the changing experimental temperature, which in turn is used to calculate equilibrium fugacity for the Englezos model.

6.3. Mole fraction in the presence of hydrate

In the Skovborg/Rasmussen model, the difference between the mole fraction of methane in the bulk liquid phase in the presence of hydrate, x_b, and at equilibrium, x_{eq}, is used as a driving force for the hydrate growth. To determine this x_b value, several steps must be followed. First, determination of the mole fraction at 1atm pressure using the formula provided by the Perry's Chemical Enginner's Handbook (Perry & Green, 1999):

$$\ln x = A + \frac{B}{T} + C \ln T + DT \tag{95}$$

Where:

A, B, C and D are constants provided for methane from the same source, and are equal to:

A = -338.217

B = 13282.1

C = 51.9144

D = -0.0425831

And T represent the experimental temperature. Knowing the mole fraction, this can be used to determine the Henry's law constant H:

$$H = \frac{1}{x} \tag{96}$$

Which in turn can be used to find the mole fraction at experimental pressure in pure water:

$$x_{Pexp} = \frac{Pexp}{H} \tag{97}$$

The final step is correcting this mole fraction based on the fact that there are hydrates present, which will alter this value slightly. There are no clear cut way to do this, but the problem was solved by the use of a diagram from the text book Clathrate Hydrate of Natural Gases (Sloan Jr & Koh, 2007) where concentration of methane in pure water is compared with concentration of methane in water with hydrates present, and then the difference was estimated by inspection of the diagram. This diagram is shown in the figure below:

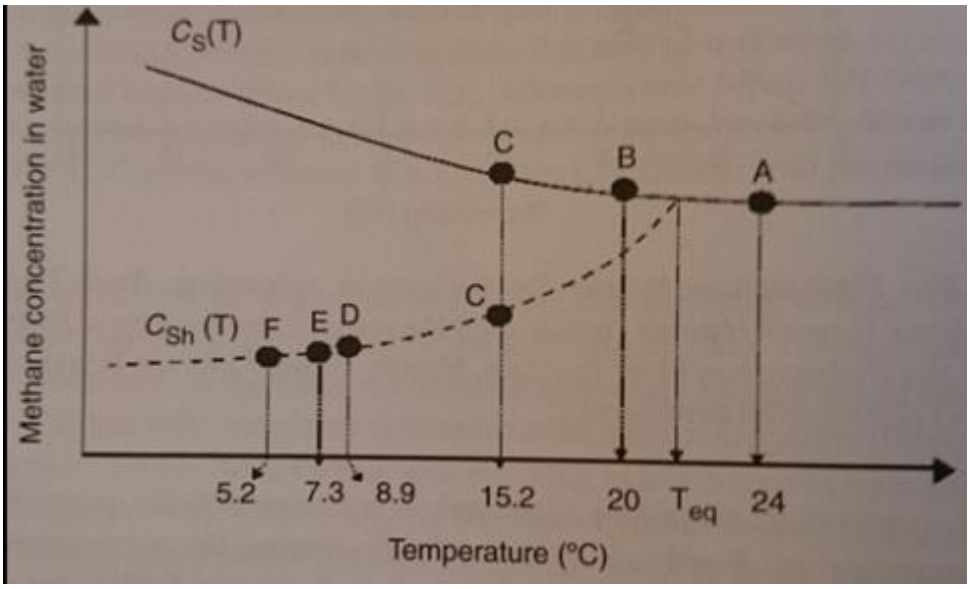

Figure 28: C_s(T) represent the concentration of methane in pure water, and C_{sh}(T) for methane in water containing hydrates.

Since the value of $C_s(T)$ is known at both experimental and equilibrium temperature, the difference between these points can be used to estimate the difference between $C_{sh}(T=eq)$ and $C_{sh}(T=exp)$, and then in turn for mole fraction.

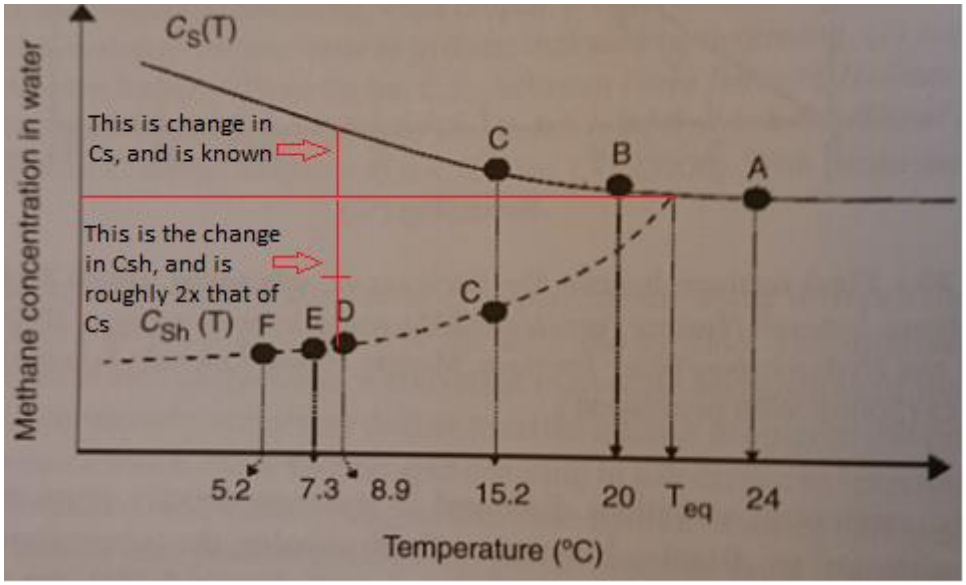

Figure 29: Shows how the change in $C_{sh}(T)$ can be estimated.

The change in concentration between equilibrium and relevant temperatures seemed to be roughly twice as big when considering hydrates present. Instead of an increasing value, a decreasing value at twice the rate can be seen. Converted to mole fractions instead of concentration:

$$x_b = x_{eq} - 2 \times (x_{Pexp} - x_{eq}) \tag{98}$$

Where x_b is the mole fraction of methane in the liquid bulk phase in the presence of hydrates, and x_{eq} is the mole fraction at equilibrium, which is the same for both pure water and water with hydrates.

6.4. Skovborg and Rasmussen Model result comparison

As expected, when the measured experimental results from stage 2 hydrate growth are plotted against the results predicted by the Skovborg and Rasmussen model using the same mass transfer coefficient for hydrate forming component they presented in their paper, the results

obtained are not very accurate. This is obviously due to the fact that this parameter needs to be fitted with the aid of experimental data:

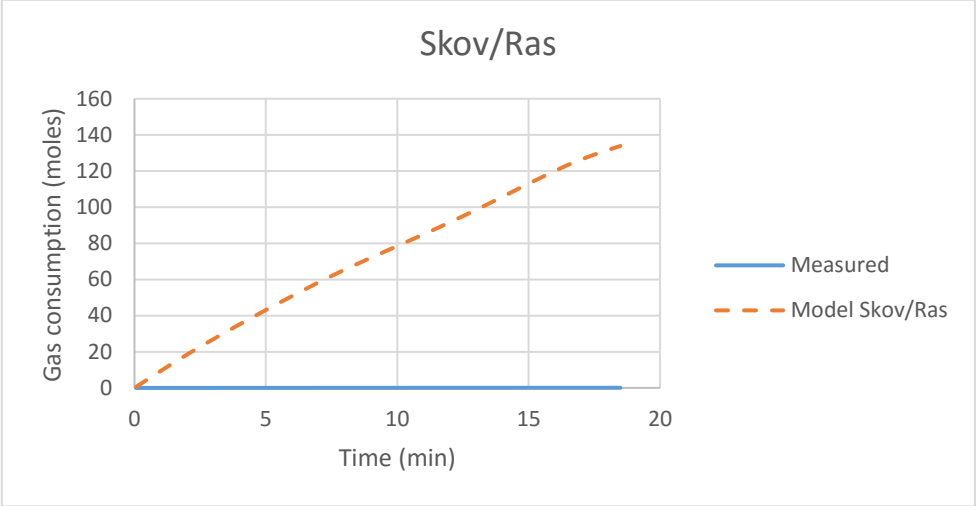

Figure 30: Shows a plot of gas consumption in a 90bar, 350 rpm and 6˚C experiment based on measured data and calculated values based on the Skovborg/Rasmussen model using initial k_L value given in the Skovborg and Rasmussen paper (Skovborg & Rasmussen, 1994).

Currently, the model overpredict the gas consumption by a lot, which means the same mass transfer coefficient, k_L, needs to be lowered:

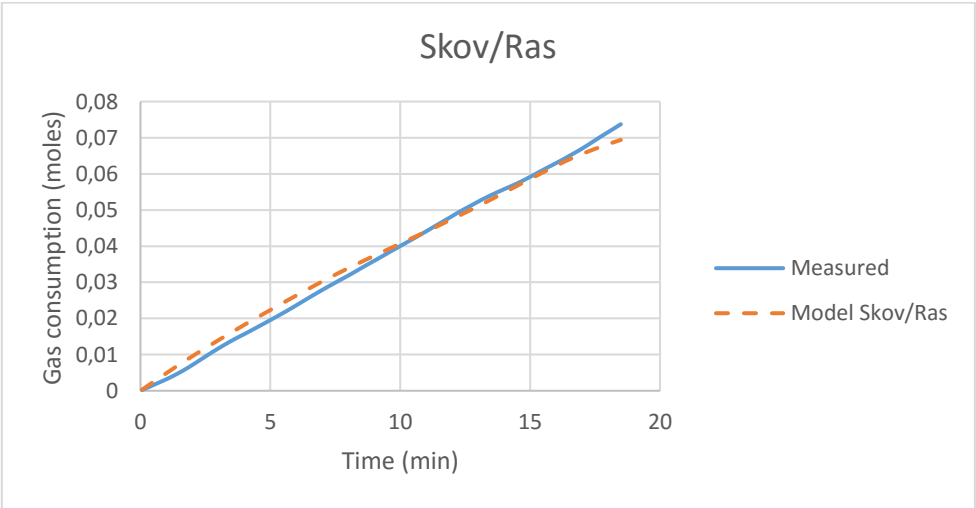

Figure 31: In this figure, the same plot is shown, but now the k_L value has been adjusted to $2.11*10^{-8}$, which results in a much higher correspondence between the two graphs.

With the k_L parameter properly fitted, the model can quite accurately be used to predict gas consumption in stage 2 hydrate growth, but starts to deviate after roughly 17 minutes after start of growth phase 2, at which point the model will underpredict the gas consumption ever so slightly.

The k_L parameter is to some minor degree sensitive to temperature changes, and more so to rpm changes. In the two tables below the values of k_L is presented with respects to appropriate temperature and stirring rate:

Table 2: Temperature dependence, values given for 575 rpm

Temperature, ˚C	k_L value, m/s
6	$2{,}21*10^{-8}$
7	$2{,}31*10^{-8}$
8	$2{,}41*10^{-8}$

Table 3: RPM dependence, values given for 6 ˚C

RPM	k_L value, m/s
225	$1{,}35*10^{-8}$
350	$2{,}11*10^{-8}$
425	$2{,}11*10^{-8}$
500	$2{,}61*10^{-8}$
575	$2{,}21*10^{-8}$
650	$2{,}12*10^{-8}$
725	$2{,}11*10^{-8}$
800	$3{,}41*10^{-8}$

From the data in the tables above, a trend can be observed where the value of k_L increases with increasing stirring rate, and slightly with increasing temperature. This trend may to some degree be a result of the changes in total gas-liquid interfacial area which in theory should be dependent on stirring rate, but was kept constant in this thesis.

As the rpm of the experiments increases, the tendency of underprediction by the model increases by a minor amount. This can be observed in the 800 rpm experiment below:

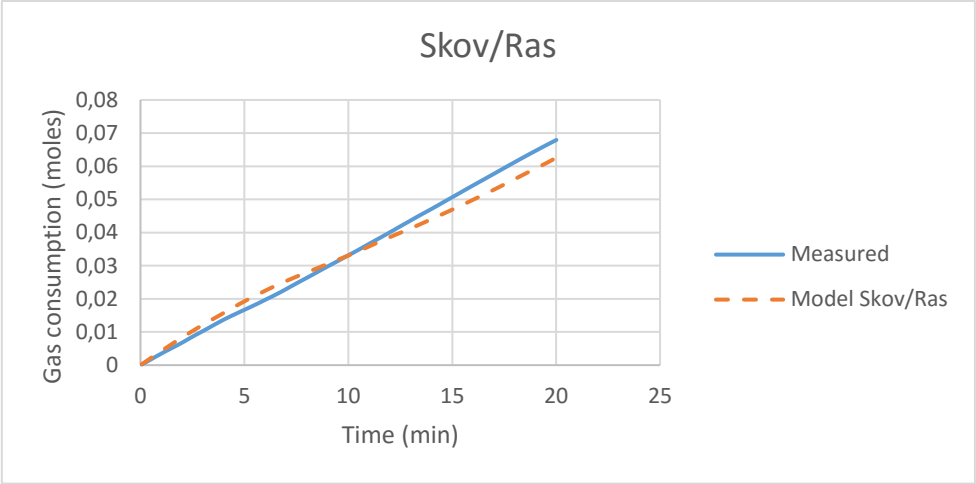

Figure 32: 800 rpm 6˚C showing how the Skovborg/Rasmussen model underpredict the gas consumption with increasing rpm.

This is most likely due to the fact that as rpm increases, the total interfacial area between the gas and liquid increases by an unknown amount. Since this is kept constant in these experiments, some deviations can be expected.

When the experimental results are compared to the ones obtained by Skovborg and Rasmussen in their experiments, a familiar trend of a slight underprediction at around the same time can be observed:

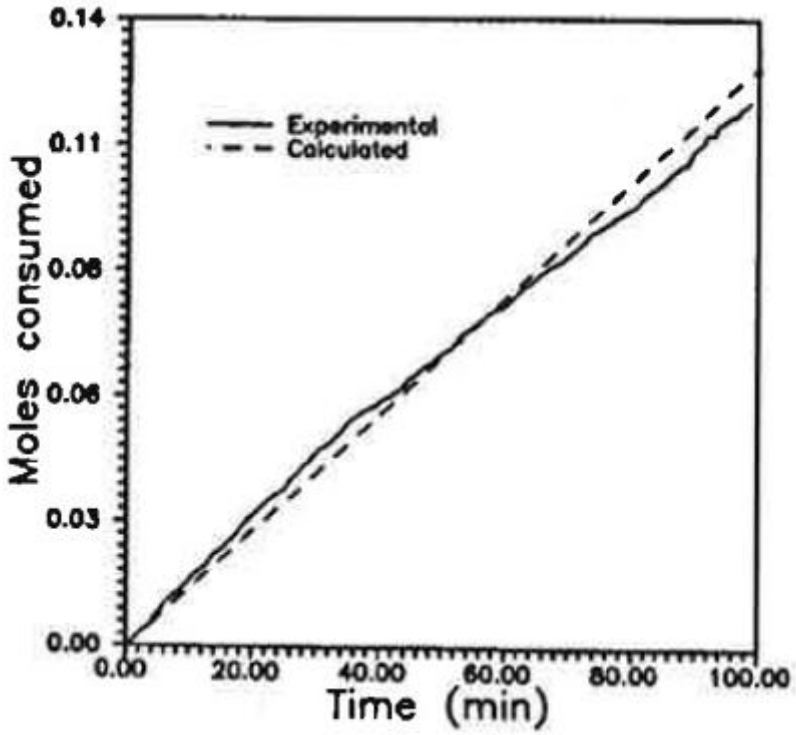

Figure 33: Comparison of experimental and calculated hydrate growth curves for methane at 6.93 MPa, 276.05K and 400 rpm (Skovborg & Rasmussen, 1994).

Their experimental setup was of course not the same as the one used in this thesis, so identical results are not expected. However, some similarities can definitely be seen.

6.5. Englezos Model result comparison

As with the Skovborg and Rasmussen mode, the Englezos produced some very satisfying results with excellent correlation between measured and calculated hydrate growth rate. First example is from the same conditions as with the first result presented for the Skovborg and Rasmussen model:

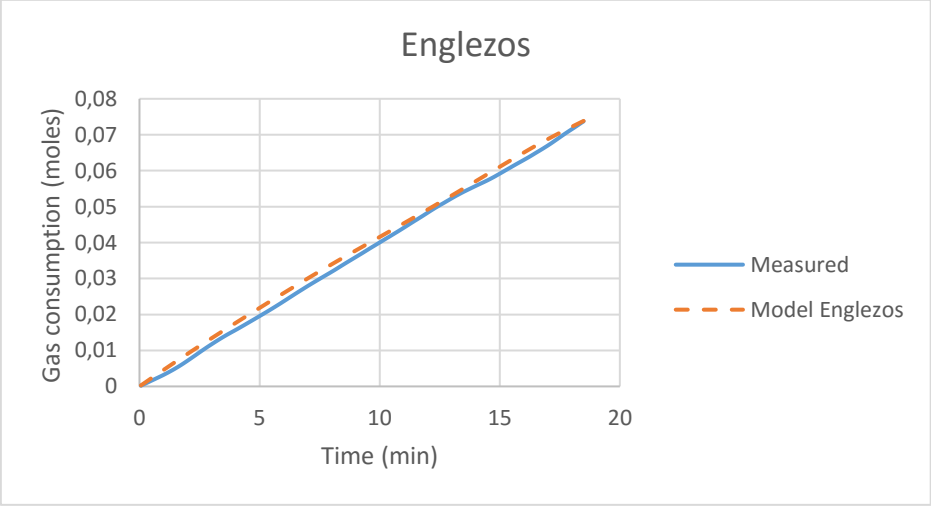

Figure 34: Shows a plot of gas consumption in a 350 rpm 6˚C experiment based on measured data and calculated values based on the Englezos model using fitted K* value.

When plotted against the measured and Skovborg and Rasmussen data:

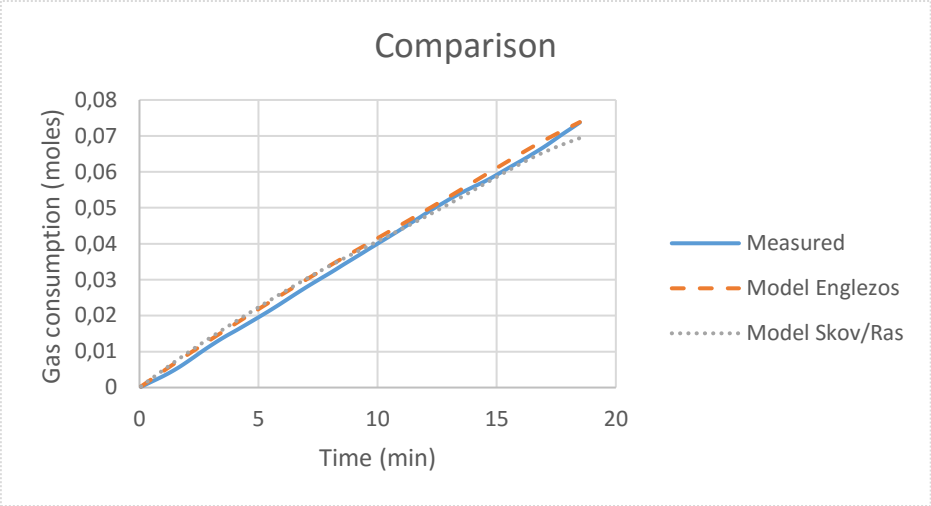

Figure 35: 350 rpm, 6˚C: plot of Englezos, Skovborg and Rasmussen and measured hydrate growth curve.

As indicated by the figure above, the three different approaches to calculate the hydrate growth rate are in good agreement with each other.

Comparing with the results presented by Englezos in his paper (Englezos et al., 1987), very similar results can be seen both in terms of actual values, and correspondence between the curves, despite the fact that the experimental setups used are different. Below is a figure of some plots from the paper showing some curves based on different pressures, the one furthest to the left, 7.60 MPa, is closest to the setup used in this thesis, which was 90 bar pressure:

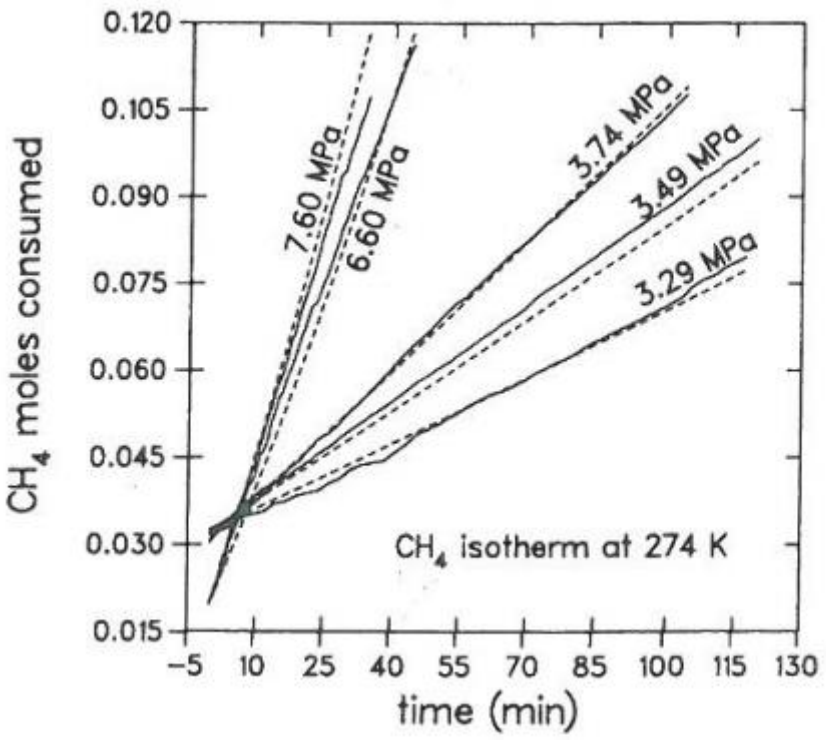

Figure 36: Dotted line (----) represent the calculated curves for methane hydrate formation, and the drawn line (—) is the experimental data. (Englezos et al., 1987)

As with the k_L parameter from the Skovborg and Rasmussen model, also the K^* value needs to be adjusted for temperature and rpm:

Table 4: Temperature dependence, values given for 575 rpm

Temperature, ˚C	K^* value, mol/m^2 s Mpa
6	$4{,}53*10^{-7}$
7	$4{,}54*10^{-7}$
8	$4{,}55*10^{-7}$

Table 5: RPM dependence, values given for 6 ˚C

RPM	K^* value, mol/m^2 s Mpa
225	$2{,}73*10^{-7}$
350	$4{,}53*10^{-7}$
425	$4{,}53*10^{-7}$
500	$5{,}03*10^{-7}$

575	$4{,}53*10^{-7}$
650	$4{,}31*10^{-7}$
725	$4{,}53*10^{-7}$
800	$4{,}93*10^{-7}$

A similar trend for K^* can be observed as with k_L, however, K^* appears to have a maximum value at 575 rpm stirring rate, as opposed to k_L. Temperature has an even less effect on the K^* value than it did on k_L.

When computing for higher rpm, such as 800 rpm, the model still gives good estimations of the gas consumption rate.

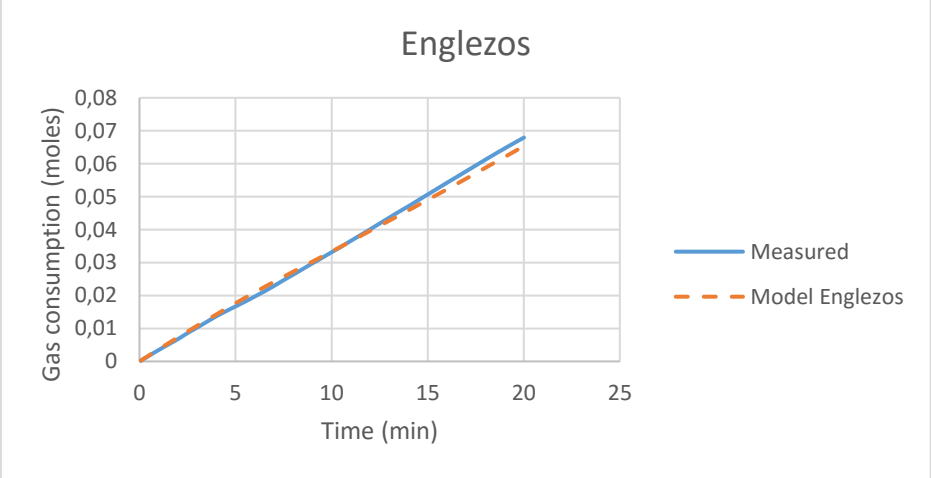

Figure 37: 800 rpm, 6˚C, plot of measured and computed hydrate growth curves.

In this case, the underprediction is so low that it is almost neglectable.

Changing the temperature in the experimental cell to 8˚C from 6˚C, has some impact on the result, with a slight increase in underprediction:

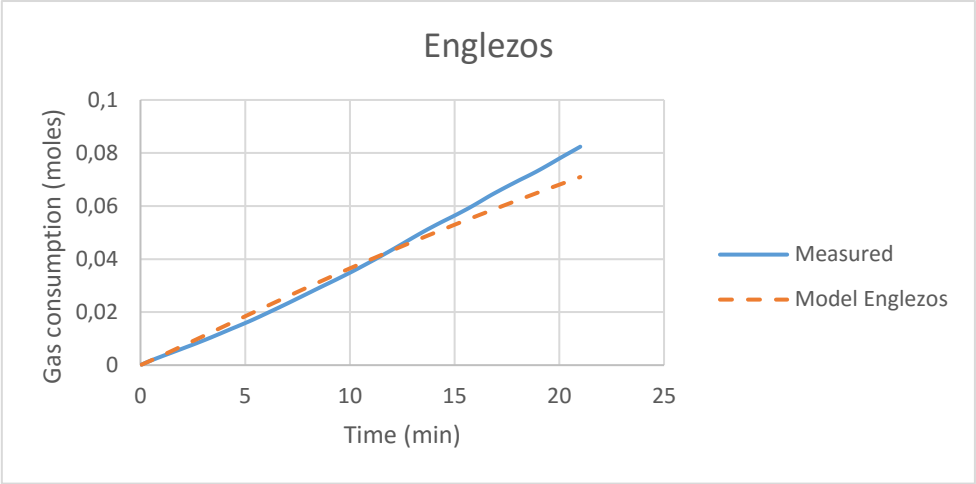

Figure 38: 575 rpm, 8˚C, and 90 bar. A plot of gas consumption per min.

More results and comparisons between model calculations and measured data are available in Appendix B.

7. CONCLUSION

The rate of gas hydrate formation was measured in a 141.4 ml stirred test cell at 90 bar pressure and experimental temperature ranging from 6 to 8˚C. This was made possible by monitoring injected gas from a separate gas supply. The stirring rates variated between 225 and 800 rpm.

Some natural gas hydrate models was analysed, with a focus on what approach the authors used to reach their results.

The data obtained from the experiments was then used to compare and analyse the kinetic growth rate constant K^* and k_L based on the models by Englezos and Skovborg and Rasmussen. The analysis showed some good correspondence between measured and estimated results, but was also ultimately limited due to lack of exact measurements of total gas-liquid interfacial area, among some other less important parameters.

A trend was found for K^* and k_L where they increase in value with increasing rpm and slightly with increasing temperature. K^* was found to have a maximum value at 575 rpm, and k_L was more heavily dependent on temperature changes.

The number one limitation that all of the models analysed have in common is that they in some sense use a growth rate constant which needs to be fitted based on experimental results, which makes them difficult to adapt to different circumstances.

8. FUTURE WORK

For an improved understanding behind the kinetics of natural gas hydrate growth, the following is recommended for future work on the subject:

- A reliable way to measure or calculate the gas-liquid interfacial area and second moment of particle size distribution as a function of stirring rate
- Improve the accuracy of the measuring apparatus.
- The goal for the ambiguous should be to discover a universal model that can describe the kinetics of hydrate growth under any given condition

REFERENCES:

Abbott, M. M., Smith, J. M., & Van Ness, H. C. (2001). Introduction to chemical engineering thermodynamics. *McGraw-Hill*.

Boer, G. B. J. D., & Hoedemakers, G. F. M. (1989). Coagulation in turbulent flow, part i. Chemical Engineering Research and Design. 301-307.

Chaudhari, R., Gholap, R., Emig, G., & Hofmann, H. (1987). Gas-liquid mass transfer in "dead-end" autoclave reactors. *The Canadian Journal of Chemical Engineering, 65*(5), 744-751.

Christiansen, R., & Sloan Jr, E. (1995). *A compact model for hydrate formation*. Retrieved from

Clarke, M. A., & Bishnoi, P. (2005). Determination of the intrinsic kinetics of CO2 gas hydrate formation using in situ particle size analysis. *Chemical Engineering Science, 60*(3), 695-709.

Davidson, D. (1973). Clathrate hydrates *Water in Crystalline Hydrates Aqueous Solutions of Simple Nonelectrolytes* (pp. 115-234): Springer.

Davy, S. H., & Bulmer, W. (1810). *On Some New Electrochemical Researches, on Various Objects, Particularly the Metallic Bodies, from the Alkalies, and Earths, and on Some Combinations of Hydrogene*: W. Bulmer and Company.

Duan, Z., & Mao, S. (2006). A thermodynamic model for calculating methane solubility, density and gas phase composition of methane-bearing aqueous fluids from 273 to 523K and from 1 to 2000bar. *Geochimica et Cosmochimica Acta, 70*(13), 3369-3386.

Englezos, P., Kalogerakis, N., Dholabhai, P., & Bishnoi, P. (1987). Kinetics of formation of methane and ethane gas hydrates. *Chemical Engineering Science, 42*(11), 2647-2658.

Froment, G., & Bischoff, K. (1979). Chemical reactor design and analysis.

Hammerschmidt, E. (1934). Formation of gas hydrates in natural gas transmission lines. *Industrial & Engineering Chemistry, 26*(8), 851-855.

Herri, J.-M., Pic, J.-S., Gruy, F., & Cournil, M. (1999). Methane hydrate crystallization mechanism from in-situ particle sizing. *AIChE Journal, 45*(3), 590-602.

Jeffrey, G. (1984). Hydrate inclusion compounds. *Journal of inclusion phenomena, 1*(3), 211-222.

Kane, S., Evans, T., Brian, P., & Sarofim, A. (1974). Determination of the kinetics of secondary nucleation in batch crystallizers. *AIChE Journal, 20*(5), 855-862.

Kashchiev, D., & Firoozabadi, A. (2002). Nucleation of gas hydrates. *Journal of crystal growth, 243*(3), 476-489.

Khamskiĭ, E. V. (1969). *Crystallization from solutions*: Consultants Bureau.

LIEVOIS, J. S. (1987). *Development of an automated, high pressure heat flux calorimeter and its application to measure the heat of dissociation of methane hydrate.* Rice University.

McMullan, R. K., & Jeffrey, G. (1965). Polyhedral clathrate hydrates. IX. Structure of ethylene oxide hydrate. *The Journal of Chemical Physics, 42*(8), 2725-2732.

Meindinyo, R.-E. T., Svartaas, T. M., Nordbø, T. N., & Bøe, R. (2015). Gas Hydrate Growth Estimation Based on Heat Transfer. *Energy & Fuels, 29*(2), 587-594.

Munck, J., Skjold-Jørgensen, S., & Rasmussen, P. (1988). Computations of the formation of gas hydrates. *Chemical Engineering Science, 43*(10), 2661-2672.

Noyes, A. A., & Whitney, W. R. (1897). The rate of solution of solid substances in their own solutions. *Journal of the American Chemical Society, 19*(12), 930-934.

Nyvlt, J., Sohnel, O., Matuchova, M., & Broul, M. (1985). *The Kinetics of Industrial Crystallization*. Amsterdam.

Perry, R. H., & Green, D. W. (1999). *Perry's chemical engineers' handbook*: McGraw-Hill Professional.

PetroWiki. (2015). Preventing formation of hydrate plugs. Retrieved from http://petrowiki.org/Preventing_formation_of_hydrate_plugs

Ramkrishna, D. (2000). *Population balances: Theory and applications to particulate systems in engineering*: Academic press.
Ribeiro, C. P., & Lage, P. L. (2008). Modelling of hydrate formation kinetics: State-of-the-art and future directions. *Chemical Engineering Science, 63*(8), 2007-2034.
Rowland, S. P., & Stillinger, F. (1980). *Water in polymers*: American Chemical Society Washington, DC.
Salmi, T. O., Mikkola, J.-P., & Warna, J. P. (2011). *Chemical reaction engineering and reactor technology*: CRC Press.
Skovborg, P., & Rasmussen, P. (1994). A mass transport limited model for the growth of methane and ethane gas hydrates. *Chemical Engineering Science, 49*(8), 1131-1143.
Sloan Jr, E. D., & Koh, C. (2007). *Clathrate hydrates of natural gases*: CRC press.
Tohidi, B. (2011). What are gas hydrates? *Heriot watt University-Institue of petroleum engineering*.
Türkmen, I. R. (2007). *Homogeneous Nucleation Rates of Ice in Supercooled Binary Liquid Mixtures of Water+ Non-electrolytes: A combined Theoretical and Experimental Study.* Freie Universität Berlin.
Volmer, M., & Weber, A. (1926). Novel growth mechanism in heteroepitaxial semiconductor growth. *Z. Phys. Chem, 119*, 277.

APPENDIX A

Fugacity calculation

All of the fugacity calculations needed for the Englezos model is presented in this section. The equations for this was obtained from the text book "Introduction to Chemical Engineering Thermodynamics" 7th edition (Abbott et al., 2001).

The first fugacity needed for the model is f_g, or the gas phase fugacity:

$$f_g = P \times \varphi_g \tag{99}$$

Where φ_g is the fugacity coefficient of the gas phase, determined by:

$$\ln \varphi_g = \frac{B_{ii}P}{RT} \tag{100}$$

Where B_{ii} in turn is found from:

$$B_{ii} = B \times R\frac{T_c}{P_c} \tag{101}$$

Where

B = second viral coefficient

T_c = critical temperature of methane

P_c = critical pressure of methane

B is found:

$$B = B^0 + \omega B^1 \tag{102}$$

$$B^0 = 0.083 - \frac{0{,}422}{T_r{}^{1.6}} \tag{103}$$

$$B^1 = 0.139 - \frac{0.172}{T_r{}^{4.2}} \tag{104}$$

Where

ω = the acentric factor, and is equal to 0.012 for methane.

T_r = the reduced temperature of methane, equal to temperature divided by critical temperature

This is quite a long process, which must be repeated when determining equilibrium fugacity coefficient φ_{eq} since it will have its respective temperature and pressure conditions. Once this is found, f_{eq} and f_b can be calculated:

$$f_{eq} = \varphi_{eq} P_{eq} \tag{105}$$

Where P_{eq} is the equilibrium pressure at the given experimental temperature, found as described in the Equilibrium Pressure section. And:

$$f_b = \varphi_{eq} P_{eq} exp \frac{V^l (P - P_{eq})}{RT} \tag{106}$$

Where V^l is the liquid-phase molar volume of water, and is assumed constant.

APPENDIX B

Experimental data

In this section experimental results and comparisons between the different approaches will be presented in curves for the different experimental conditions. Not every single experiment run have their result listed here, but a diversified selection is representing many different stirring rates and temperatures, with some identical experimental runs to indicate accuracy. The results are listed in terms of rate of stirring, temperature in cell, number of identical experimental run, all are for 90 bar pressure:

225 rpm, 6˚C, #1:

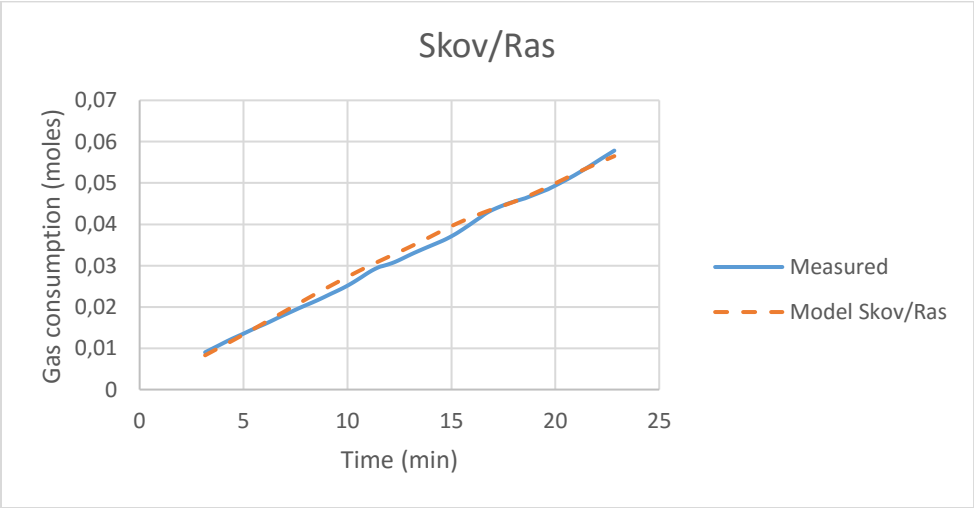

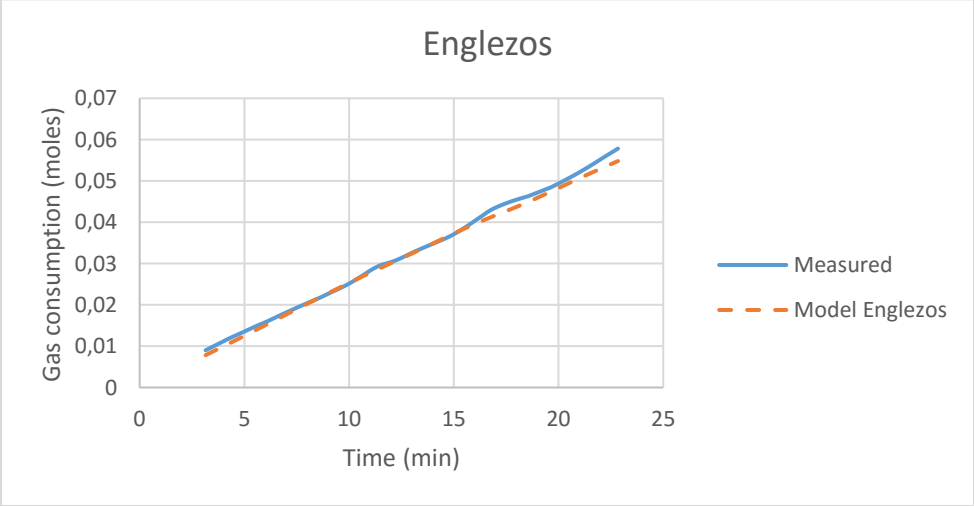

225 rpm, 6˚C, #2:

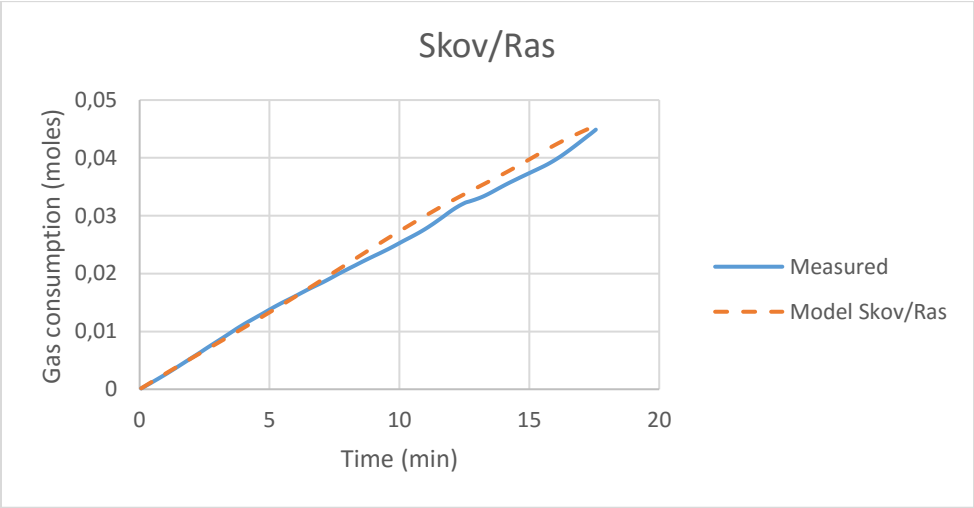
Skov/Ras
Gas consumption (moles)
0,05
0,04
0,03
0,02
0,01
0
0
5
10
15
20
Time (min)
Measured
Model Skov/Ras

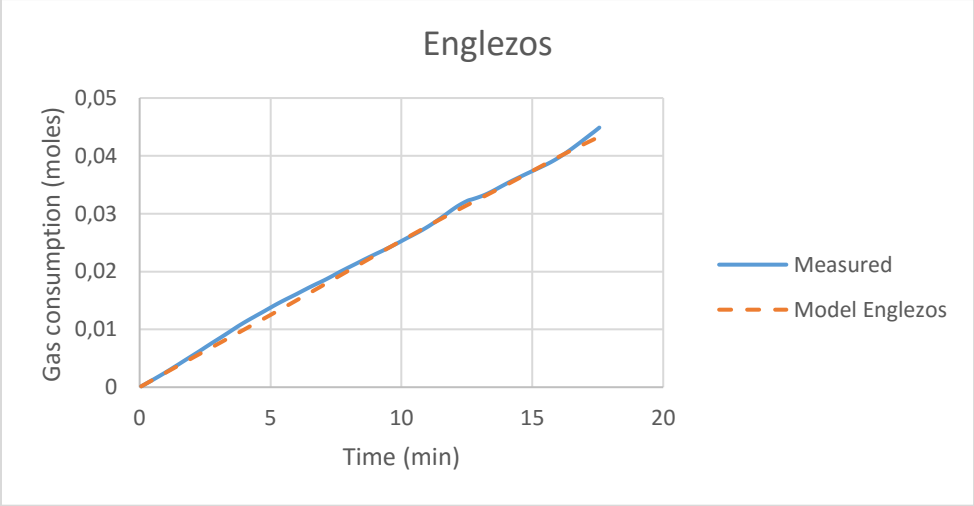
Englezos
Gas consumption (moles)
0,05
0,04
0,03
0,02
0,01
0
0
5
10
15
20
Time (min)
Measured
Model Englezos

350 rpm, 6˚C, #1:

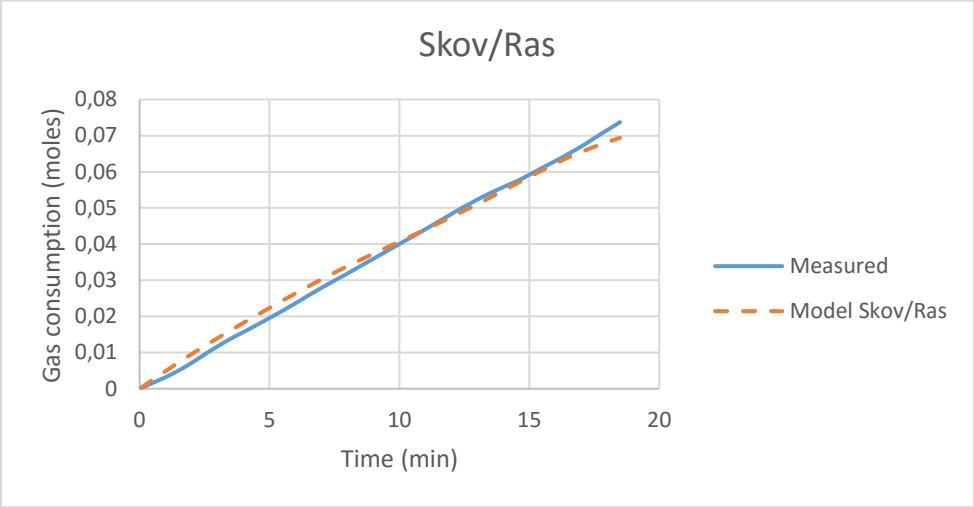

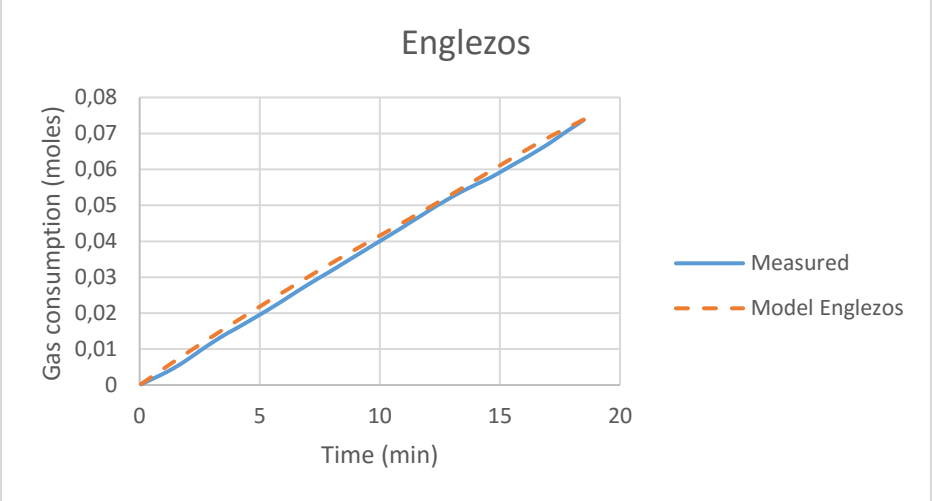

425 rpm, 6˚C, #5:

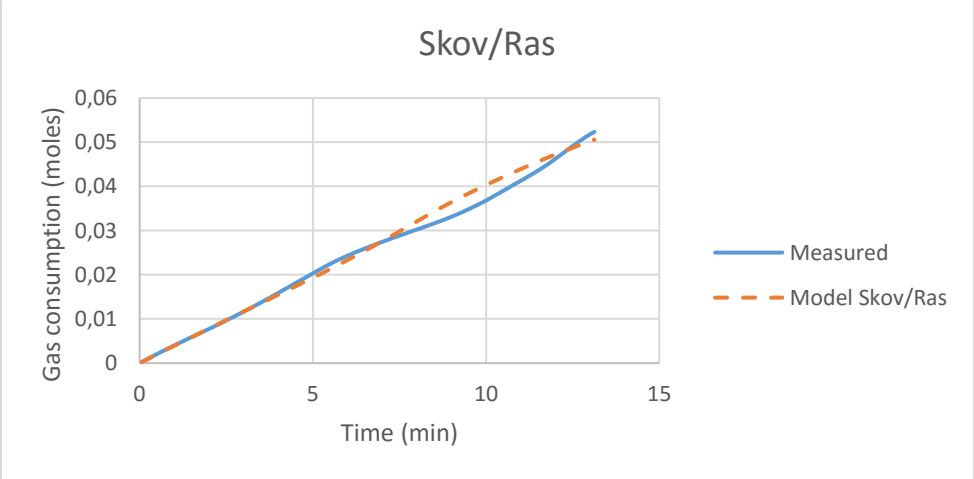

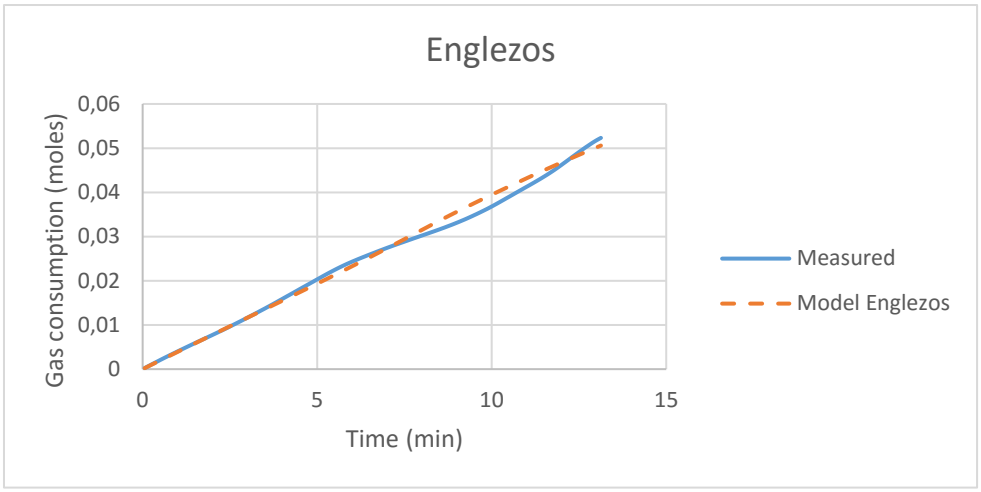

500 rpm, 6˚C, #1:

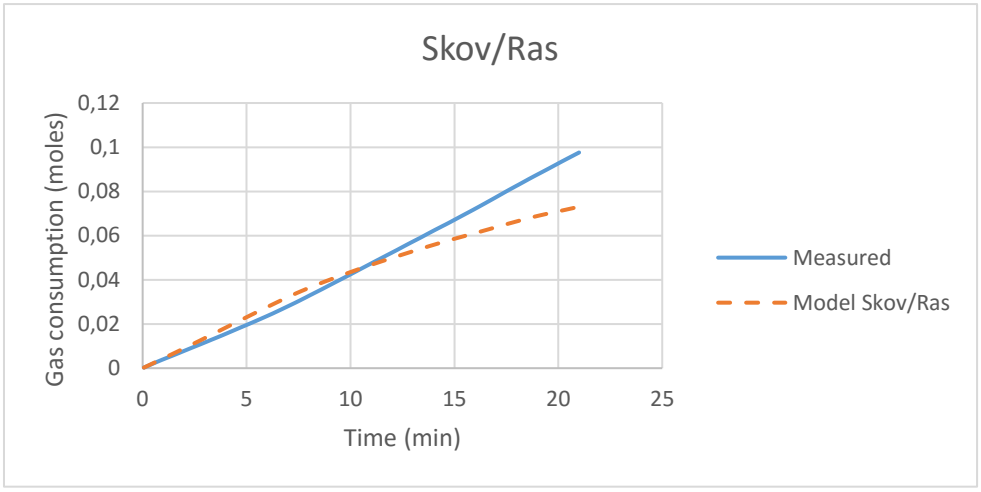

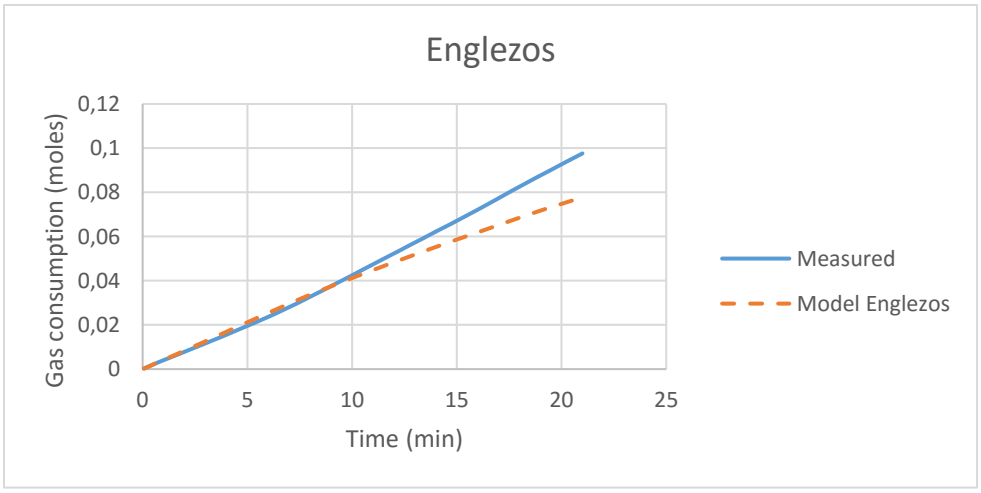

575 rpm, 6˚C, #1:

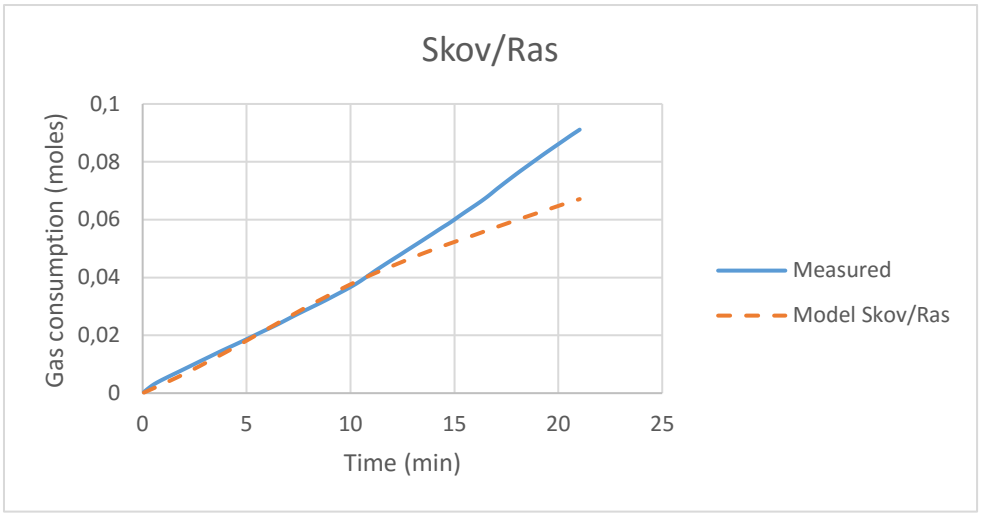
Skov/Ras
Gas consumption (moles)
0,1
0,08
0,06
0,04
0,02
0
0
5
10
15
20
25
Time (min)
Measured
Model Skov/Ras

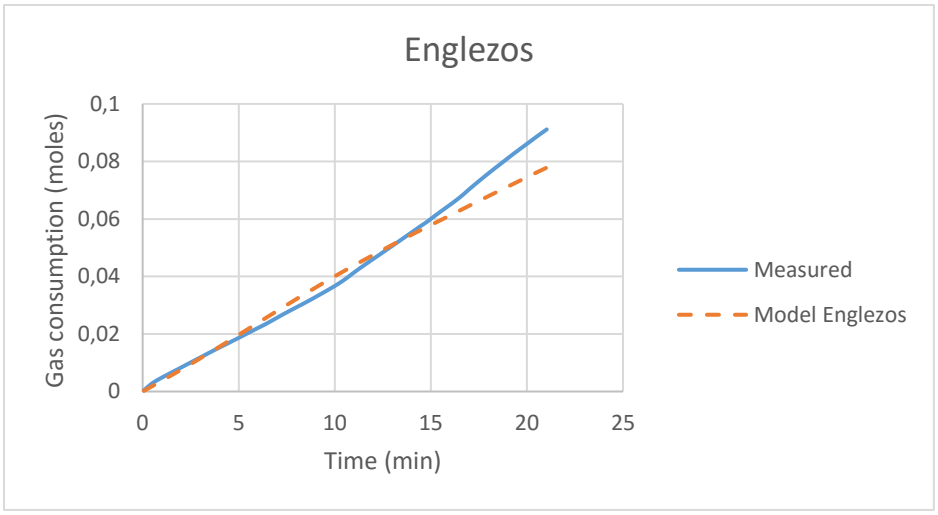
Englezos
Gas consumption (moles)
0,1
0,08
0,06
0,04
0,02
0
0
5
10
15
20
25
Time (min)
Measured
Model Englezos

575 rpm, 6˚C, #2:

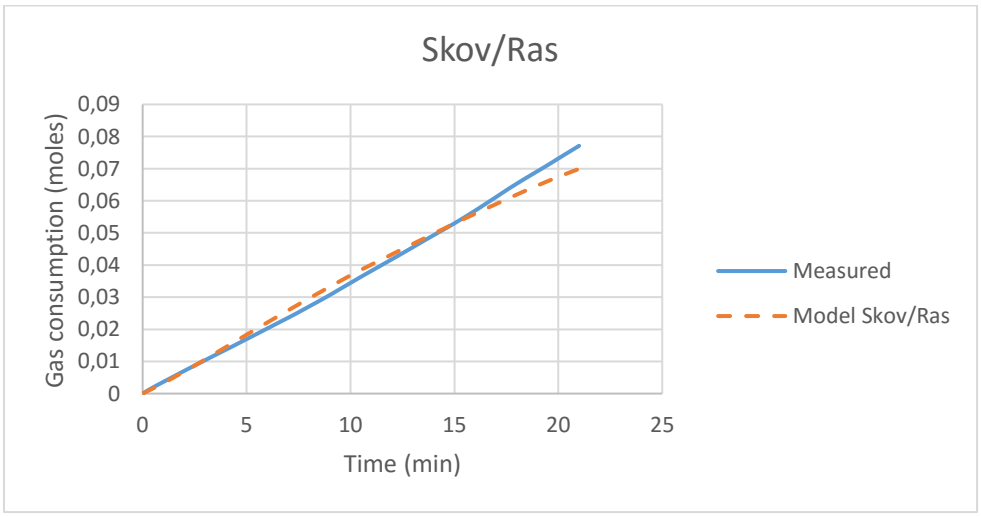
Skov/Ras
Gas consumption (moles)
0,09
0,08
0,07
0,06
0,05
0,04
0,03
0,02
0,01
0
0
5
10
15
20
25
Time (min)
Measured
Model Skov/Ras

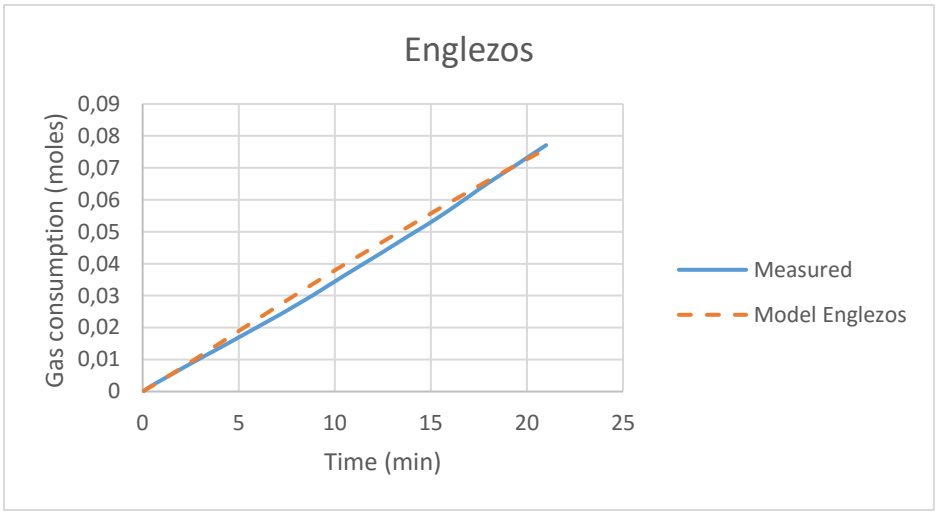

575 rpm, 7˚C, #1:

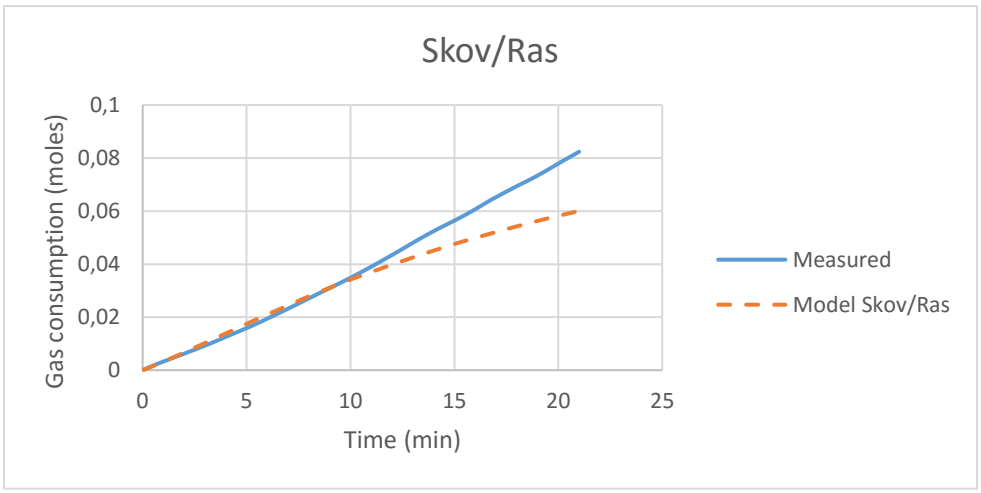

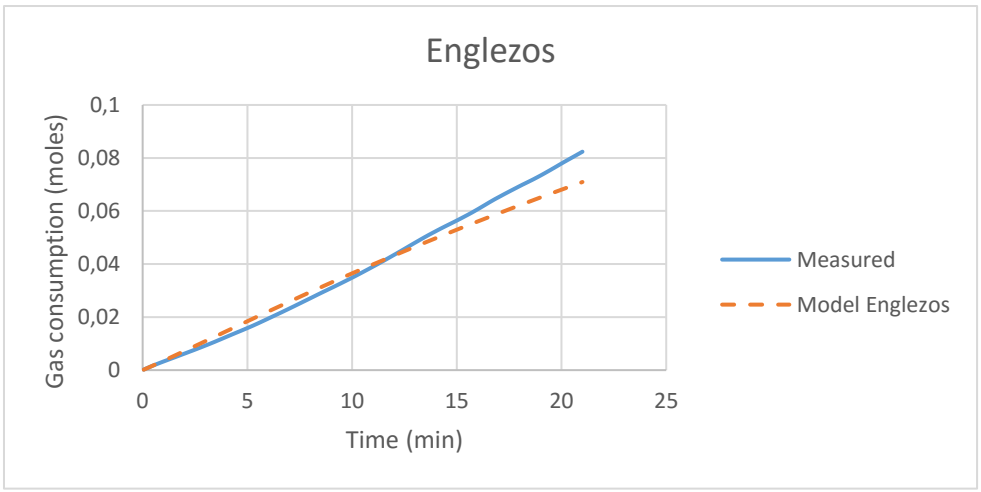

575 rpm, 8˚C, #1:

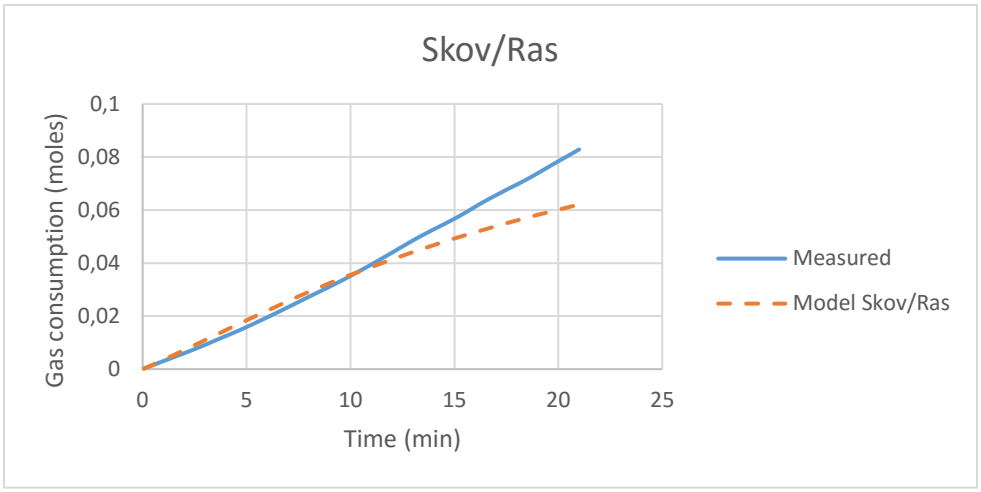
Skov/Ras
Gas consumption (moles)
0,1
0,08
0,06
0,04
0,02
0
0
5
10
15
20
25
Time (min)
Measured
Model Skov/Ras

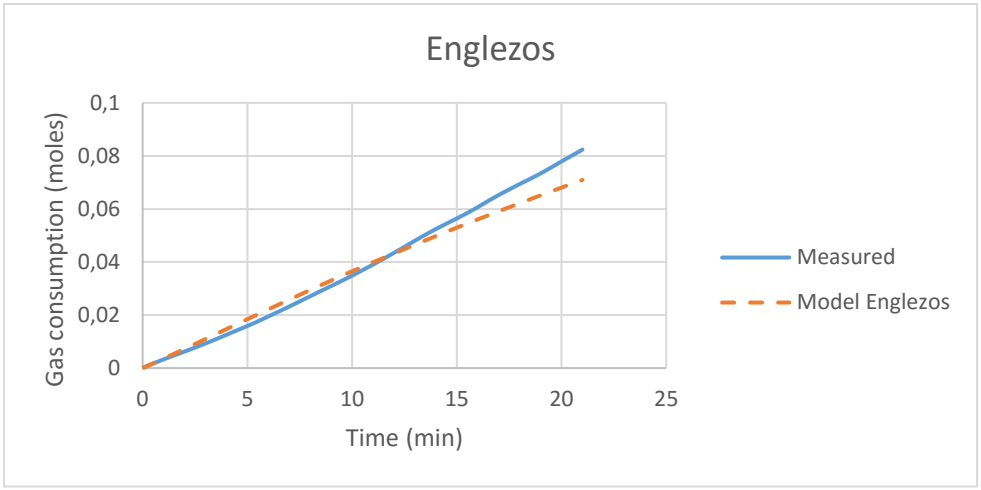
Englezos
Gas consumption (moles)
0,1
0,08
0,06
0,04
0,02
0
0
5
10
15
20
25
Time (min)
Measured
Model Englezos

650 rpm, 6˚C, #1:

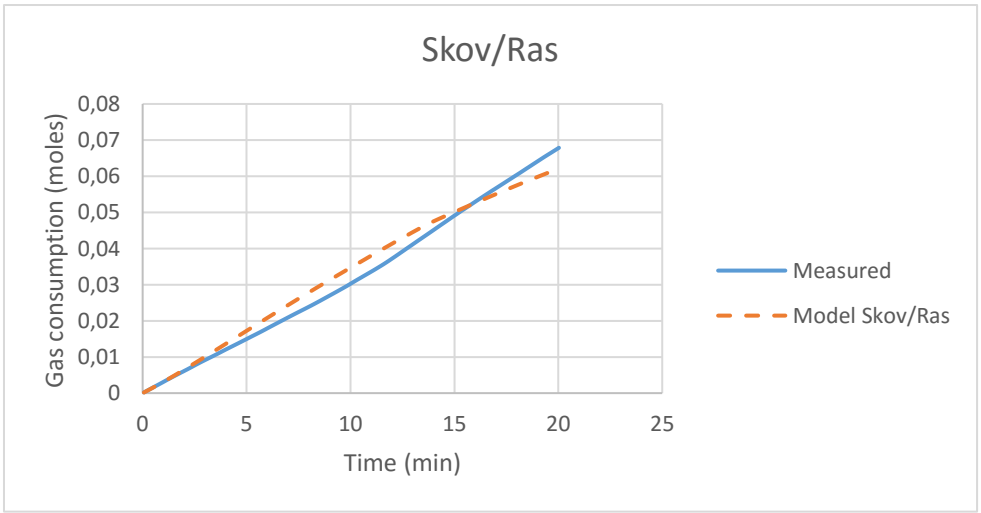
Skov/Ras
Gas consumption (moles)
0,08
0,07
0,06
0,05
0,04
0,03
0,02
0,01
0
0
5
10
15
20
25
Time (min)
Measured
Model Skov/Ras

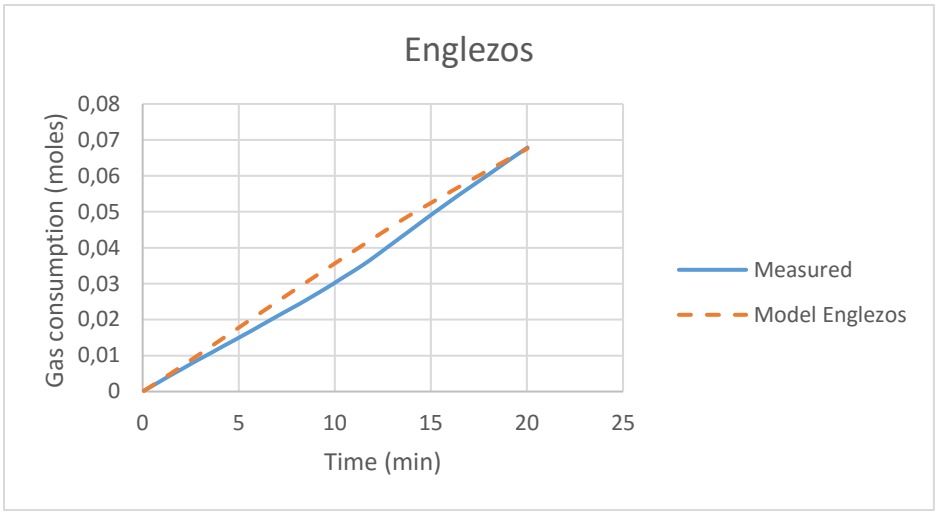

725rpm, 6˚C, #1:

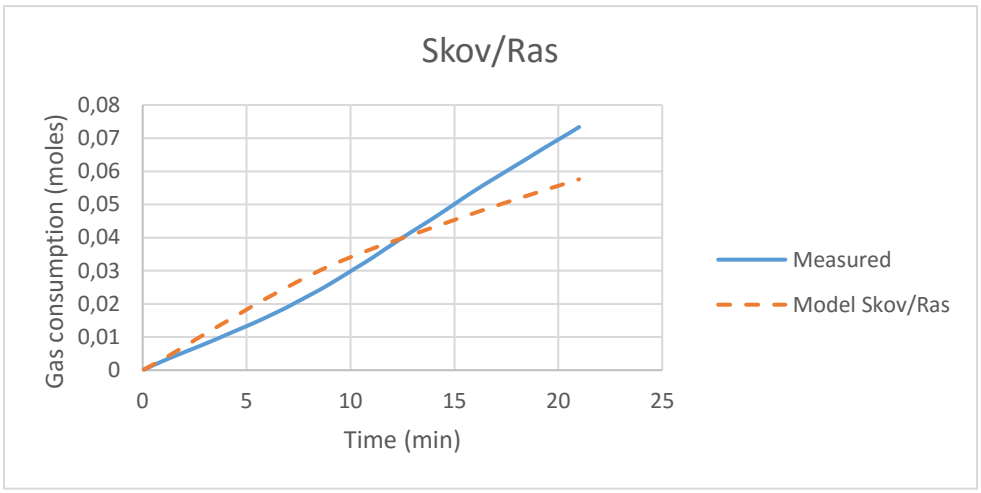

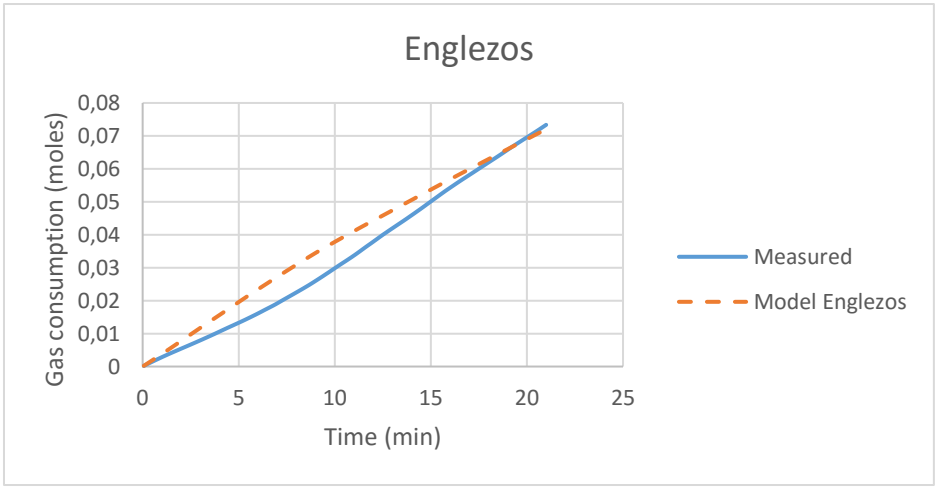

800 rpm, 6˚C, #1:

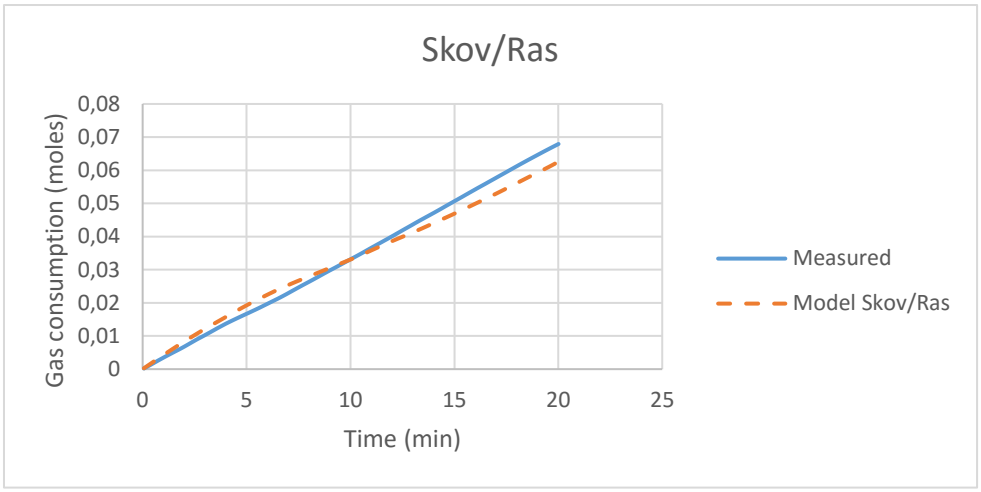
Skov/Ras
Gas consumption (moles)
0,08
0,07
0,06
0,05
0,04
0,03
0,02
0,01
0
0
5
10
15
20
25
Time (min)
Measured
Model Skov/Ras

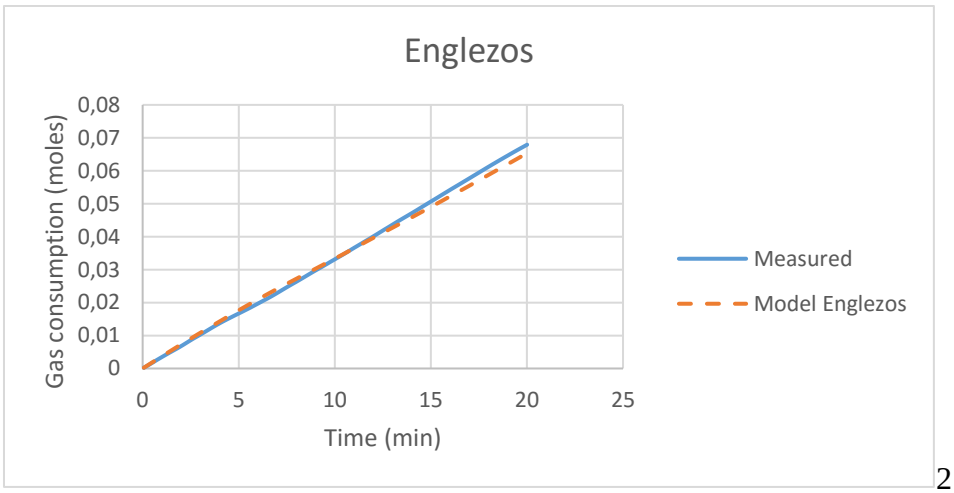
Englezos
Gas consumption (moles)
0,08
0,07
0,06
0,05
0,04
0,03
0,02
0,01
0
0
5
10
15
20
25
Time (min)
Measured
Model Englezos

2